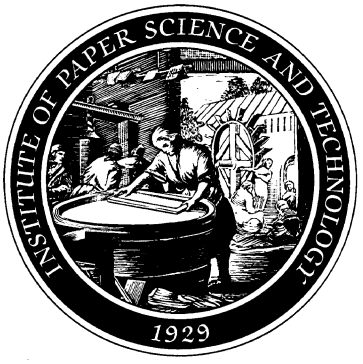

Institute of Paper Science and Technology
Atlanta, Georgia

IPST Technical Paper Series Number 646

A Theoretical Model of Flotation Deinking Efficiency

F. Bloom and T.J. Heindel

March 1997

Submitted to
Journal of Colloid and Interface Science

INSTITUTE OF PAPER SCIENCE AND TECHNOLOGY
PURPOSE AND MISSIONS

The Institute of Paper Science and Technology is a unique organization whose charitable, educational, and scientific purpose evolves from the singular relationship between the Institute and the pulp and paper industry which has existed since 1929. The purpose of the Institute is fulfilled through three missions, which are:

- to provide high quality students with a multidisciplinary graduate educational experience which is of the highest standard of excellence recognized by the national academic community and which enables them to perform to their maximum potential in a society with a technological base; and
- to sustain an international position of leadership in dynamic scientific research which is participated in by both students and faculty and which is focused on areas of significance to the pulp and paper industry; and
- to contribute to the economic and technical well-being of the nation through innovative educational, informational, and technical services.

ACCREDITATION

The Institute of Paper Science and Technology is accredited by the Commission on Colleges of the Southern Association of Colleges and Schools to award the Master of Science and Doctor of Philosophy degrees.

NOTICE AND DISCLAIMER

The Institute of Paper Science and Technology (IPST) has provided a high standard of professional service and has put forth its best efforts within the time and funds available for this project. The information and conclusions are advisory and are intended only for internal use by any company who may receive this report. Each company must decide for itself the best approach to solving any problems it may have and how, or whether, this reported information should be considered in its approach.

IPST does not recommend particular products, procedures, materials, or service. These are included only in the interest of completeness within a laboratory context and budgetary constraint. Actual products, procedures, materials, and services used may differ and are peculiar to the operations of each company.

In no event shall IPST or its employees and agents have any obligation or liability for damages including, but not limited to, consequential damages arising out of or in connection with any company's use of or inability to use the reported information. IPST provides no warranty or guaranty of results.

A Theoretical Model of Flotation Deinking Efficiency

Frederick Bloom* and Theodore J. Heindel+

* Department of Mathematical Sciences, Northern Illinois University, DeKalb, IL 60115

\+ Engineering and Paper Materials Division, Institute of Paper Science and Technology, 500 10th St., N.W., Atlanta, GA 30318

Suggested Running Title: Theoretical Model of Flotation Deinking

Name/Address for Correspondence:

Professor Theodore J. Heindel
Institute of Paper Science and Technology
500 10th St., N.W.
Atlanta, GA 30318-5794

Abstract

The associated probabilities of each microprocess occurring in flotation deinking are employed in the development of a kinetic or population balance-type model of the overall flotation process. The overall model contains two kinetic constants: The first, k_1, governs the overall probability of a free ink particle successfully being intercepted by and adhering to an air bubble; the second, k_2, is a measure of the probability that a particle/bubble aggregate pair will become unstable and split to yield a "new" free ink particle.

The solution to the kinetic model is presented in terms of k_1 and k_2, which are themselves functions of system parameters such as bubble and particle physical properties (e.g., diameter, density), fluid properties (e.g., viscosity, surface tension), etc. From this solution, a definition of a theoretical flotation efficiency, as well as other system performance parameters, are presented, and selected predictions are displayed.

Key Words: flotation deinking, kinetic model, probability of adhesion, probability of detachment, sliding, three-phase contact, disjoining film, critical film thickness, collision frequency, turbulent energy density.

INTRODUCTION

Flotation deinking is a separation process in which swarms of small air bubbles rise through agitated liquid tanks with suspended cellulose pulp and contaminant particles; the bubbles preferentially attach to naturally or chemically hydrophobized contaminant and ink particles, carrying them to a froth layer at the surface of the tank, where they are removed. Although the flotation technique has been widely used in the mineral processing industry for more than a century, during the past 30 to 50 years, it has been adapted for the separation of ink particles, toner particles, and contaminants from cellulose fibers for the recycling of wastepaper products.

Modern flotation cell designs vary with respect to their geometry, operating parameters, and flow configurations. In Fig. 1 we depict the Black Clawson IHI/BC flotation cell, a unit which injects gas via two turbines at the bottom of the cell, thus inducing very effective mixing. A more detailed description of flotation deinking equipment, which contains descriptions of other types of deinking cells, can be found in recent review articles (1), (2). Despite the differences among various flotation deinking systems, they all operate on similar principles and incorporate the three basic processes of aeration of the pulp, mixing to maximize bubble-particle interaction, and separation of bubble-particle aggregates from the bulk mixture. The survey paper (3) is a good source for early efforts at modelling flotation processes in the mineral processing industry; more recent efforts are discussed only in the monograph (4); what emerges from these (and similar) accounts in the literature is that the overall flotation separation process has been treated as a multistage probability process, which is tied to the view of the overall flotation process as being a sequence of microprocesses. Initially, surfactants are added to the pulp mixture in a flotation cell so that the surfaces of the particles become hydrophobic, thus facilitating attachment of those particles to the

air bubbles introduced into the cell by the aeration process. The sequence of microprocesses referred to, above, include the approach of a particle to an air bubble, with the subsequent interception of that particle by the bubble, the sliding of the particle along the surface of the thin liquid film which separates the particle from the bubble, film rupture, with the subsequent formation of a three-phase contact between the bubble, particle, and film, and the stabilization of the particle/bubble aggregate and its subsequent transport to the froth layer for removal. Many authors (e.g., (5)) have, even recently, noted the need for models to combine the elementary microprocesses occurring in a flotation deinking cell into a coherent mathematical model of the overall process.

The simple model, which we present in this paper, is more in line with the formulation of logistic population growth models, as opposed to the simple exponential-type population growth models, which may be found in many places in the literature (e.g., (3), (4), (6)). Transport balance models, which involve not only time variations in particle concentration due to particle/bubble aggregate formation and destruction, but also account for convection and diffusion processes in a unit volume of a flotation cell, thereby leading to partial differential equations instead of ordinary differential equations, have recently been discussed only in general terms in (7).

In the overall flotation deinking process, the interception of a particle by a bubble can take place only if the trajectory of the particle is within a streaming tube of radius R_c (Fig. 2), the so-called capture radius; expressions for R_c vary according to whether one models the flow around a particular bubble as Stokes flow, potential flow, or some flow intermediate to these. During the sliding process, the disjoining film which separates a particle from a bubble, may thin down to a critical thickness where rupture of the film occurs with the subsequent development of the three-phase contact, which we have already alluded to; in

this situation, a certain minimal time, the induction time τ_i, is required in order for the disjoining film to thin down to the point where rupture can occur. If $\tau_{s\ell}$ represents the sliding time of the particle, then we must have $\tau_{s\ell} \geq \tau_i$ and, in addition, adhesion by sliding must occur for a touching angle ϕ_T (see Fig. 2) in the range $0 < \phi_T < \frac{\pi}{2}$. Finally, once an ink particle successfully adheres to a particle, the particle/bubble aggregate will experience stresses during its elevation into the froth layer, which tend to destabilize that aggregate. Critical to the stability or instability of a particle/bubble aggregate is the ratio of the adhesive forces F_{ad} between the particle and the bubble to the detachment forces F_{det} (which depend, in a crucial manner, on how one models the acceleration generated in the turbulent flow field in the cell). Among the other forces which act on an aggregate in the flotation cell are the force of gravity, the static buoyancy force of the immersed part of the bubble, the hydrostatic pressure of the liquid above the contact area of the particle at the fluid interface between the particle and bubble after formation of the three-phase contact, the capillary force exerted on the three-phase contact, and the capillary pressure in the gas bubble which acts on the contact area of an attached particle. The ratio of detachment forces F_{det} to attachment forces F_{ad}, which characterizes the stability of the aggregate, turns out to be a (dimensionless) similarity parameter, analogous to the so-called Bond number (8).

In the next section we offer a description of the probability distributions which can be associated to the key microprocesses we have described above.

THEORY I: MICROPROCESS PROBABILITIES

We begin with the delineation of suitable expressions for R_c (Fig. 2), the radius of the limiting streaming tube within which a particle must move in order to be intercepted by a bubble and the associated interception probability P_c; henceforth, all particles and bubbles in any given volume element of the flotation cell will be assumed to be perfectly spherical.

The type of expression one obtains for R_c depends critically on the basic assumptions made about (i) the relative sizes R_p and R_B of particles and bubbles, respectively, and (ii) the nature of the flow field in which the particle moves. Inertial forces play little or no role for particles removed by flotation deinking, which tend to follow, with little deviation, the fluid streamlines in the flow field around a bubble; the interception probability for such particles is, therefore, much lower than those of mineral-type size. A key quantity in discussing the flow field in the neighborhood of a bubble is the bubble Reynolds number $Re_B = v_B d_B \rho_\ell / \mu_\ell$, where v_B is the bubble rising velocity, $d_B = 2R_B$ the bubble diameter, ρ_ℓ the liquid density in the cell, and μ_ℓ the dynamic viscosity of that liquid. A constant C_B is used by several authors (e.g., (8), (9), (10)) to characterize the degree of bubble retardation, which results from having the surface of a bubble covered by a surfactant, with $C_B = 1$ corresponding to a completely retarded or rigid bubble. Another important quantity associated with the determination of P_c is the Stokes number

$$St = \rho_p d_p^2 v_B / 9\mu_\ell d_B \equiv Re_B \rho_p d_p^2 / 9\rho_\ell d_B^2 \qquad [1]$$

which represents the ratio of the inertia force of a particle to the viscous drag force of the bubble; in [1] $d_p = 2R_p$ while ρ_p is the particle density. For typical (ink) particles, $St << 0.1$, and, as we have indicated above, inertia forces do not influence particle motion, thus ruling out impact collisions between particles and bubbles.

If we define P_c to be the ratio of the number of particles with $R_p < R_B$, which encounter a bubble per unit time, to the number of particles which approach a bubble in a stream tube with cross-sectional area πR_B^2, then $P_c = (R_c/R_B)^2$. At this stage of approach of a particle to a bubble we consider only long-range hydrodynamic interactions as opposed to those short-range interactions which must be taken into account in the sliding process (discussed

below). If one takes into account those forces which act on a particle as it approaches a single bubble in the flotation cell, namely, the drag force, gravitational force, and buoyancy force, lets $\vec{v}_p$ (with components v_{px} and v_{py}) represent the particle velocity, (see Fig. 3) and utilizes the inertial mass of the particle (i.e., the actual particle mass plus the mass of the fluid accelerated with it), then the following system of equations is obtained (4):

$$\frac{4}{3}\pi R_p^3 \rho_p \frac{dv_{px}}{dt} = -\frac{4}{3}\pi R_p^3 \Delta\rho g - 6\pi\mu_\ell R_p(v_{px} - u_x) \qquad [2]$$

$$\frac{4}{3}\pi R_p^3 \rho_p \frac{dv_{py}}{dt} = 6\pi\mu_\ell R_p(u_y - v_{py}) \qquad [3]$$

where $\vec{u}$ is the velocity field of the liquid in a neighborhood of the bubble. If we write [2] and [3] in dimensionless form, then the key parameters that appear are the Stokes number St, as given in [1], and the dimensionless particle settling velocity

$$G = 2R_p^2(\rho_p - \rho_\ell)g/9\mu_\ell v_B \qquad [4]$$

An expression for R_c is now based on the solution of an initial value problem for the system [2], [3] coupled with assumptions about the nature of the velocity field $\vec{u}$, the magnitudes of the key parameters, and information about the degree of retardation of the bubble surface (because normal and tangential components of the fluid flow around the bubble surface are dependent on the degree of bubble surface retardation). For actual flotation machines, several authors have pointed out that bubble Reynolds numbers in the range $1 < Re_B < 100$ apply; in which case, following Yoon and Luttrell (11), we have the following expression for the radial and tangential components of the velocity field $\vec{u}_*$ of the liquid

$$u_{*r} = u_{rs} - v_B \frac{3Re_B^*}{2}\left(\frac{R_B^4}{r^4} - \frac{R_B^3}{r^3} - \frac{R_B^2}{r^2} - \frac{R_B}{r}\right)\cos\phi \qquad [5]$$

$$u_{*\phi} = u_{\phi s} + v_B \frac{3Re_B^*}{4}\left(\frac{R_B}{r} + \frac{R_B^3}{r^3} - \frac{2R_B^4}{r^4}\right)\sin\phi \qquad [6]$$

where

$$Re_B^* = Re_B^{0.72}/15 \qquad [7]$$

and $u_{rs}, u_{\phi s}$ are the radial and tangential components of the velocity field for a Stokes flow around the bubble, i.e., (12)

$$u_{rs} = -v_B\left(1 - \frac{(2\mu_\ell + 3\eta)}{2(\mu_\ell + \eta)}\frac{R_B}{r} + \frac{\eta R_B^3}{2(\mu_\ell + \eta)r^3}\right)\cos\phi \qquad [8]$$

$$u_{\phi s} = v_B\left(1 - \frac{(2\mu_\ell + 3\eta)}{4(\mu_\ell + \eta)}\frac{R_B}{r} - \frac{\eta R_B^3}{4(\mu_\ell + \eta)r^3}\right)\sin\phi \qquad [9]$$

with η a coefficient depending on the mobility of the bubble surface.

From the system [2], [3] with associated initial conditions, and the expressions for the fluid velocity field, estimates have been developed for R_c; for the case in which $St << 0.1$, Dukhin et al. (12), Derjaguin et al. (13), Ahmed and Jameson (14), and Yoon and Luttrell (11) have derived, for rigid bubbles ($C_B = 1$), bubble sizes up to 1 mm, and intermediate range Reynolds numbers, the expression

$$P_c = \left(\frac{3}{2} + \frac{4Re_B^{0.72}}{15}\right)\frac{R_p^2}{R_B^2} \qquad [10]$$

which is thought to be valid for particle sizes up to 100 μm. However, one must be cognizant of the fact that any expression, such as [10], for P_c, is dependent on the degree of bubble retardation as well as other factors in the cell.

The next critical process in the overall flotation deinking scheme is the sliding of a particle along the surface of the thin liquid film surrounding the bubble with a resultant weak surface deformation; here, the contact time of the particle with the liquid film is critical as it must be larger than the drainage (or induction) time of the film up to the point of rupture. To estimate the probability of adhesion by sliding, $P_{as\ell}$, one must model the motion of a particle, in the flow field of the bubble, as it slides over the surface of the disjoining film, in order to predict the film thickness h as a function of the positional angle ϕ. The probability $P_{as\ell}$ depends strongly on the critical film thickness h_{crit}, the assumptions one makes about the flow field around the bubble, the degree of mobility of the bubble surface, the particle and bubble sizes, and the bubble rising velocity. Among the common assumptions in the literature are the following (8), (9):

(i) the particles move in a quasistationary manner (i.e., inertial forces are negligible) on an almost circular path across the bubble surface.

(ii) the sliding path L is much greater than the film thickness h, and moreover, it is assumed that $dL/dt > dh/dt$.

(iii) in the domain $0 < \phi < \pi/2$, the influence of the flow boundary layer is negligible, especially in the case of movable or unretarded bubbles.

(iv) the tangential component of the fluid flow can, as in the computation of P_c, be modeled in the case of an unretarded bubble by potential flow and in the case of a completely retarded bubble by the intermediate flow of Yoon and Luttrell (11).

The force balance governing the sliding motion of an ink particle may be obtained from Fig. 4; in particular, in polar coordinates, balance of forces in the radial and tangential directions assume the forms

$$-F_{gr} - F_{ur} + F_T + F_c + F_L = 0 \qquad [11]$$

and

$$F_{g\phi} - F_{w\phi} = 0 \qquad [12]$$

where F_{gr} is the component of the (apparent) particle weight in the radial direction; F_T is the resistive force generated during the drainage of the liquid film surrounding the bubble surface; F_c is the centrifugal force acting on the sliding particle which (by assumption) moves on a circular path with radius $r = R_B + R_p + h$ (h the disjoining film thickness); F_{ur} is the 'flow force' which acts on the sliding particle close to the bubble wall; F_L is the drainage (or lift) force acting on the particle; $F_{g\phi}$ is the component of the (apparent) particle weight in the tangential direction; and $F_{w\phi}$ is the drag force acting on the particle. The drag force is strongly dependent on both the nature of the flow field as well as the degree of retardation of the bubble surface. Also, F_T must be estimated by using the theory of capillary hydrodynamics for thin films. Expressions for all of the forces delineated above may be found in, e.g., (8), where it is assumed, in particular, that $F_T = 6\pi\mu_\ell R_p^2 v_{pr}/hC_B$; such an expression, in turn, follows from taking the capillary pressure P_σ caused by the deformation of the bubble surface to have the form

$$P_\sigma = \frac{\sigma}{x}\frac{\partial}{\partial x}\left(x\frac{\partial h_1}{\partial x}\right) \qquad [13]$$

with h_1 (see Fig. 5) weakly time-dependent and σ the surface tension. The function h_1 measures the warping of the bubble surface at x, where x is the radial coordinate in a local polar coordinate system within the dimple on the bubble surface (see the Appendix and Fig. 14a); it is assumed that $\partial h_1/\partial x << 1$. For $h_1(x)$, Derjaguin et al. (15) obtain the equation

$$\frac{\partial^3 h_1}{\partial x^3} + \frac{1}{x}\frac{\partial^2 h_1}{\partial x^2} - \frac{1}{x^2}\frac{\partial h_1}{\partial x} = \frac{3}{2\sigma}\mu_\ell v_{pr} f(x) \qquad [14]$$

with

$$f(x) = x\left(h_1(0) + \hat{h} + \frac{x^2}{2R_p}\right)^{-3}, \qquad [15]$$

$\hat{h}$ the distance between the particle and the nondeformed bubble surface; one also has the associated boundary data

$$\left.\frac{\partial h_1}{\partial x}\right|_{x=0} = \lim_{x\to\infty}\frac{\partial h_1}{\partial x} = 0 \qquad [16]$$

From [14], [15], [16], one may generate an expression for $h_1(x)$ whose use in the integral

$$F_T = \iint P_\sigma dS_B \equiv 2\pi\sigma\int_0^\infty \frac{\partial}{\partial x}\left(x\frac{\partial h_1}{\partial x}\right)dx \qquad [17]$$

serves to generate the aforementioned result for F_T when $C_B = 4$. The expression [13] for P_σ may be generalized to account specifically for the London-Van der Waals dispersion and electrostatic interaction effects on surface tension (16), (17). Alternatively, for the overall film thickness $h(x,t)$, where x now represents the arc length along the bubble surface to a fixed point on the bubble surface (see the Appendix and Fig. 14b), Williams and Davis (16) obtain

$$\frac{\partial h}{\partial t} = \frac{1}{3\mu_\ell}\frac{\partial}{\partial x}\left[h^3\left(\frac{\partial P_\sigma}{\partial x}\right)\right] \qquad [18]$$

the particular nonlinear partial differential equation with results being dependent on the expression adopted for P_σ. In the Appendix, we indicate how [14] and [18] are just different local coordinate realizations of the same basic partial differential equation. When the surface concentration of surfactant varies within the cell, one must, in fact, deal not only with a

generalization of [18] to cover the case of a variable surface tension, i.e., $\frac{\partial \sigma}{\partial x} \neq 0$, but must also couple to that extended equation a transport equation for the surface concentration of surfactant Γ, where $\sigma = \sigma_0 + M\Gamma$ and $M = \sigma'(\Gamma)$ may be assumed to be constant; details related to such an extension may be found in Paulsen et al. (17).

From the balance of forces equations (11), (12), and expressions for the individual forces which are depicted in Fig. 4, a system of the form

$$\frac{d\phi}{dt} = F_1(\phi, h); \ \frac{dh}{dt} = F_2(\phi, h) \qquad [19]$$

with associated initial data

$$\phi(0) = \phi_T; \ h(0) = h_0 \qquad [20]$$

may be obtained for the pair (ϕ, h), where $\phi(t)$ gives the location along the bubble surface, at time t, for the particle with touching angle $\phi_T = \phi(0)$, and $h(t)$ is the height of the disjoining film above that point on the bubble surface at the same time t. Eliminating the time variable in [19], one obtains an equation of the form

$$\frac{dh}{d\phi} = F(\phi, h), \qquad [21]$$

for the variation of the disjoining film thickness with the position angle, and the associated initial condition that $h = h(0) \equiv h_0$, for $\phi = \phi(0) \equiv \phi_T$, (see Fig. 6). The critical position angle ϕ^*_{crit} is now defined to be the largest touching angle ϕ_T which can be used in the system [13], [14] so that $h = h_{crit}$ will be reached at a position angle ϕ_{crit} such that $\phi_T < \phi_{crit} < \frac{\pi}{2}$; the relationship that exists among ϕ_T, h_{crit}, and ϕ^*_{crit} is depicted in Fig. 7, and the probability of adhesion by sliding is now defined by (Schulze (8))

$$P_{as\ell} = \sin^2 \phi^*_{crit} \qquad [22]$$

While the structure of the system [19], [20] is known to be such that only numerical solutions are possible, it has been determined [10] that $P_{as\ell}$ (i) increases as R_B increases, (ii) increases as v_B decreases, (iii) decreases as R_p increases, especially for small values of R_p, (iv) increases as C_B increases, and (v) increases as h_{crit} increases. Experimental results correlating the degree of particle hydrophobicity with h_{crit} of the form

$$h_{crit} = 23.3\,[\sigma(1 - \cos\theta_A)]^{0.16}\,, \qquad [23]$$

where θ_A is the advancing contact angle, have been reported in the literature (10), but such results are usually obtained for particular cases and cannot be used in general.

After the rupture of the thin liquid film which surrounds a bubble, a sufficiently large three-phase contact (TPC) between the film, particle, and bubble (Fig. 8) must be formed in a sufficiently short time τ_{tpc}.

The importance of the time interval τ_{tpc} is this: within the flotation cell, external stress forces will exert themselves on particle/bubble aggregates as a consequence of the existence of turbulent vortices; the formation of a sufficiently large TPC in a sufficiently short time τ_{tpc} is required so that a requisite strong force of attachment will exist to prevent dissolution of the aggregate. As a consequence of these considerations, for stable attachment after film rupture, we must have $\tau_{tpc} < \tau_v$, where τ_v is an average lifetime for turbulent vortices within the flotation cell.

For the probability of extension of the three-phase contact, Schulze (8) uses an exponential distribution of the (approximate) form

$$P_{tpc} \approx 1 - \exp\left(-\frac{\tau_v}{\tau_{tpc}}\right) \quad [24]$$

In most of the elementary kinetic or population models that have been formulated prior to this study, P_{tpc} does not enter into the product of individual probabilities that constitute the relevant kinetic constants because P_{tpc} is, to within 1 %, equal to one over a wide range of particle sizes for particles with a smooth boundary (8); we will make that same assumption in the model formulated in this paper.

In order for a particle/bubble aggregate to remain a stable entity on its journey to the froth layer, the attachment which has formed between a particle and a bubble must be stronger than the sum of all the external forces acting on the aggregate. It, therefore, becomes necessary to consider the force balance that applies to the particles at the liquid/bubble interface in order to compute P_{stab}, the probability of particle/bubble aggregate stability; the force balance (see Fig. 9) includes

$$F_g = \frac{4}{3}\pi R_p^3 \rho_p g, \quad [25]$$

the gravitational force which acts on an ink particle,

$$F_b = \frac{\pi}{3} R_p^3 \rho_\ell g \left[(1 - \cos\omega)^2 (2 + \cos\omega)\right], \quad [26]$$

the static buoyancy force acting on the immersed portion of a particle (ω being the angle indicated in Fig. 8 - so that $\omega = \pi$ for a completely immersed particle),

$$F_{hyd} = \pi R_p^2 (\sin^2\omega) \rho_\ell g z_0, \quad [27]$$

the hydrostatic pressure of the liquid of height z_0 above the contact area of radius $r_p = R_p \sin\psi \equiv R_p \sin\omega$,

$$F_{ca} = -2\pi R_p \sigma \sin\omega \sin(\omega + \theta) \qquad [28]$$

the capillary force exerted on the three-phase contact in the z-direction, θ being the contact angle,

$$F_\sigma = \pi r_p^2 P_\sigma \approx \pi R_p^2 \sin^2\omega \left(\frac{2\sigma}{R_p} - 2R_B\rho_\ell g\right) \qquad [29]$$

the force generated by the capillary pressure in the gas bubble which acts on the contact area of the attached (spherical) particle, and

$$F_d = \frac{4}{3}\pi R_p^3 \rho_p a_c \qquad [30]$$

the additional detaching force which is due to the acceleration experienced in the turbulent external flow field in the flotation cell. Expressions for a_c in [30] depend on the structure and intensity of the flow field; for aggregates in which particle size is much smaller than bubble size, it has been shown (8) that

$$a_c \approx 1.9\epsilon^{2/3}/(R_B + R_p)^{1/3} \qquad [31]$$

where ϵ is the turbulent energy dissipation in a given volume element of the flotation cell.

With $F_{ad} = F_{ca} + F_{hyd}$ denoting the sum of the attachment forces, and $F_{det} = F_g - F_b + F_d + F_\sigma$ denoting the sum of all those forces that can lead to detachment of a particle from a bubble, we now characterize the stability of a particle/bubble aggregate by the ratio

$$Bo' = \frac{F_{det}}{F_{ad}} = \frac{F_g - F_b + F_d + F_\sigma}{F_{ca} + F_{hyd}}, \qquad [32]$$

a dimensionless similarity parameter analogous to the Bond number; employing [25]-[32] it is easy to see that Bo' depends on $R_B, R_p, \rho_p, \epsilon, g, \sigma, \omega$, and θ, and approximate expressions may be found, e.g., in (8). If one now takes into account the recent experiments of Plate (18), then a reasonable form for P_{stab} is given by

$$P_{stab} = 1 - \exp\left(1 - \frac{1}{Bo'_m}\right) \qquad [33]$$

where Bo'_m is given by [32], with $F_{hyd} \approx 0$, and F_{ca} can be replaced by the maximal capillary force exerted on the three-phase contact, i.e., by

$$F_{cam} = 2\pi\sigma R_p \sin\left(\pi - \frac{\theta}{2}\right) \sin\left(\pi + \frac{\theta}{2}\right) \qquad [34]$$

THEORY II: THE KINETIC MODEL

We denote by $n_p(t)$ the total number of both free and attached ink particles in a volume element $\mathcal{V}_f$, of the flotation cell, at time t, by $n_B(t)$ the total number of bubbles in $\mathcal{V}_f$ at time t, by $n_p^f(t)$ the number of free ink particles in $\mathcal{V}_f$ at time t, by $n_p^a(t)$ the number of ink particles in $\mathcal{V}_f$ at time t which are attached to bubbles, by $n_B^f(t)$ the number of bubbles in $\mathcal{V}_f$ at time t which have no ink particles attached to them, and by $n_B^a(t)$ the number of bubbles in $\mathcal{V}_f$ at time t which have one or more ink particles attached to them. If $\bar{\lambda}(t)$ denotes the average number of ink particles at time t in $\mathcal{V}_f$ that are attached to bubbles in $\mathcal{V}_f$, then

$$n_p^a(t) = \bar{\lambda}(t) n_B^a(t) \qquad [35]$$

with $\bar{\lambda}(t) \geq 1$, for all $t \geq 0$. Although bubbles which have particles attached to them in $\mathcal{V}_f$ will, in general, have more than just one particle attached as they move toward the froth layer, and although it may be anticipated that both $\dot{n}_B(t) \neq 0$ and $\dot{n}_p(t) \neq 0$, because of

convection and diffusion of ink particles and bubbles into and out of $\mathcal{V}_f$, in this first effort we will assume that both $n_p(t) = n_p$ (const.) and $n_B(t) = n_B$ (const.), that $\bar{\lambda}(t) = 1$ for $t \geq 0$, and that $n_B \geq n_p$; many of these restrictions will be relaxed in future work. Setting $\gamma(t) = n_p^f(t)/n_p$ yields $n_p^a(t) = (1 - \gamma(t))n_p$ and, in a similar fashion, if $\gamma(t) = n_B^f(t)/n_B$, then $n_B^a(t) = (1 - \gamma(t))n_B$, for all $t \geq 0$. Clearly, the ideal situation in a flotation deinking cell would be to have, in each volume element $\mathcal{V}_f, \gamma(t) \to 0$, as $t \to \infty$, i.e., to have all the particles be attached to bubbles as $t \to \infty$.

Kinetic (or population growth) type models for the evolution of the number of particles in a volume element of a flotation cell go back (at least) to the work of Woodburn (3) and Sutherland (19), and the text (4) contains many references to work on elementary mathematical models of the flotation process. However, as Schulze has pointed out (4) "the generalized transport balance equation for flotation is still unsolved since it contains terms which cannot be expressed explicitly yet"; he presents as the generalized transport balance equation for flotation equations of the form

$$-\frac{\partial}{\partial t}(m_v \mu_i) = div\left[m_v \mu_i \vec{v_i}\right] - div\left[D_i \text{ grad } (m_v \mu_i)\right] - G_i \qquad [36]$$

where $\frac{\partial}{\partial t}(m_v \mu_i)$ is the change with time of the mass of the i-th particle class in the volume element under consideration; m_v is the total particle mass in the volume elements; μ_i is the mass fraction of the i-th class in the volume elements; $m_v \mu_i \vec{v_i}$ is the convective flow of mass of the i-th class in the volume elements; $\vec{v_i}$ is the transport velocity of the i-th class in the volume element; D_i is the diffusion coefficient of the i-th class in the volume element; D_i grad $(m_v \mu_i)$ is the diffuse mass flow of the i-th class in the volume element; and G_i is the change of mass due to aggregate formation or destruction. In flotation deinking, we have $i = 1, 2$ with $i = 1$ referring to free (ink) particles and $i = 2$ referring to (ink) particles which

adhere to bubbles; none of the models which have appeared, thus far, take into account, explicitly, the change in the number of free ink particles in $\mathcal{V}_f$ due to aggregate destruction, an issue that is dealt with in the model we now describe.

The kinetic equation in $\mathcal{V}_f$ has the form

$$\frac{dn_p^f}{dt} = -k_1 n_p^f n_B^f + k_2 n_B^a \qquad [37]$$

with

$$k_1 = zP_cP_{as\ell}P_{tpc}P_{stab}, \quad k_2 = 1 - P_{stab} \qquad [38]$$

In [37] the presence of n_B^f reflects the assumption that only a bubble with no attached particle is available to capture a particle; in [38] various expressions may be adopted for the collision frequency z some of which have the form

$$z = \Gamma_z \left(R_p + R_B\right)^\lambda \epsilon^\mu n_p n_B \qquad [39a]$$

for some positive constants Γ_z, λ, and μ, e.g., from the work of Saffman and Turner (20) it follows that $\lambda = 3,\ \mu = 1/2,\ \Gamma_z = (8\pi/15\nu_\ell)^{1/2}$, while from that of Camp and Stein (21) we have $\lambda = 3, \mu = 1/2$, and $\Gamma_z = \frac{4}{3}\nu_\ell^{-\frac{1}{2}} (\nu_\ell = \mu_\ell/\rho_\ell)$. However, Liepe and Möckel (22) address the possibility that collisions may occur between members of different species, which is a more realistic condition when considering flotation separation; the work presented in (22) leads to a collision frequency that has the form

$$z = \frac{5}{3} 2^{7/9} n_p n_B \frac{\epsilon^{4/9}}{\nu_\ell^{1/3}\rho_\ell^{2/3}} \left(R_p + R_B\right)^2 \sqrt{R_B^{14/9}(\Delta\rho_B)^{4/3} + R_p^{14/9}(\Delta\rho_p)^{4/3}} \qquad [39b]$$

where $\Delta\rho_B = \rho_B - \rho_\ell$ and $\Delta\rho_p = \rho_p - \rho_\ell$.

Using $n_B^f = n_B - n_B^a$ and $n_B^a = n_p^a$ in [37], we obtain

$$\frac{dn_p^f}{dt} = -k_1 n_B n_p^f + n_p^a(k_1 n_p^f + k_2) \qquad [40]$$

However, for all $t > 0, n_p^a = n_p - n_p^f$, so [40] yields

$$\frac{dn_p^f}{dt} = -k_1(n_p^f)^2 + [k_1(n_p - n_B) - k_2]n_p^f + k_2 n_p \qquad [41]$$

or, in view of the definition of $\gamma(t)$

$$\dot{\gamma}(t) = -(k_1 n_p)\gamma^2(t) + [k_1(n_p - n_B) - k_2]\gamma(t) + k_2 \qquad [42]$$

Setting $\alpha \equiv n_p - n_B < 0$, $A \equiv k_1 n_p > 0$, $B \equiv \alpha k_1 - k_2 < 0$, and $C \equiv k_2 > 0$ and replacing $\gamma(t)$ by $\Gamma(t) = -\gamma(t)$, we obtain

$$\dot{\Gamma}(t) = A\left[(\Gamma(t) + \frac{B}{2A})^2 - \mu^2\right] \qquad [43]$$

where $\mu^2 \equiv \frac{B^2}{4A^2} + \frac{C}{A}$ and the associated initial condition is

$$\Gamma(0) = -n_p^f(0)/n_p \qquad [44]$$

If, finally, we set $y(t) \equiv \Gamma(t) + B/2A$, we are led to the initial-value problem in $\mathcal{V}_f$:

$$\begin{cases} \dot{y}(t) = A\left[y^2(t) - \mu^2\right], \ t > 0 \\ y(0) = -\dfrac{n_p^f(0)}{n_p} + \dfrac{B}{2A} \end{cases} \qquad [45]$$

In view of the definitions, above, of A, B, and C, it is easy to check that

$$y(t) = -\frac{n_p^f(t)}{n_p} + \frac{[(n_p - n_B)k_1 - k_2]}{2n_p k_1} \qquad [46]$$

$$y(0) \equiv y_0 = \frac{(n_p - n_B)k_1 - k_2}{2n_p k_1} - \frac{n_p^f(0)}{n_p} \qquad [47]$$

and

$$\mu = \sqrt{\frac{[(n_p - n_B)k_1 - k_2]^2}{4n_p^2 k_1^2} + \frac{k_2}{n_p k_1}} \qquad [48]$$

and as $k_1, k_2 > 0$, and $n_p < n_B$, we have that $y_0 < 0$. From [38] and our discussion of the microprocess probabilities, it follows that k_1 and k_2 may be determined in terms of all the measurable or computable basic parameters of the flotation process, namely, $R_p, R_B, \theta, \epsilon, \sigma, \rho_\ell, \rho_p, \mu_\ell, h_{crit}$, etc.

An integration of [45] yields, for $t > 0$,

$$\ln \left| \frac{\zeta - \mu}{\zeta + \mu} \right| \Bigg]_{\zeta = y_0}^{\zeta = y(t)} = 2\mu A t \qquad [49]$$

We now make the (tentative) assumption that $y^2(t) > \mu^2$, for $t \geq 0$, set $\beta_0 = (y_0 - \mu)/(y_0 + \mu)$ and solve [49] for $y(t)$ so as to obtain

$$y(t) = \mu \frac{1 + \beta_0 e^{2\mu A t}}{1 - \beta_0 e^{2\mu A t}}, \quad t \geq 0 \qquad [50]$$

As $y_0 < 0$, and $\mu > 0$, clearly $y_0 - \mu < 0$. Also, because $A > 0$ and $B < 0$

$$y_0 + \mu = -\gamma(0) + \frac{|B|}{2A} + \mu \qquad [51]$$

But

$$\begin{cases} \mu = \sqrt{\dfrac{B^2}{4A^2} + \dfrac{C}{A}} > \dfrac{|B|}{2A} \\ \mu = \sqrt{\dfrac{B^2}{4A^2} + \dfrac{C}{A}} < \dfrac{|B|}{2A} + \sqrt{\dfrac{C}{A}} \end{cases} \qquad [52]$$

so

$$-\gamma(0) < y_0 + \mu < -\gamma(0) + \sqrt{\frac{C}{A}} \qquad [53]$$

If $\sqrt{\frac{C}{A}} < \gamma(0)$, i.e., if

$$\frac{n_p^f(0)}{\sqrt{n_p}} > \sqrt{\frac{k_2}{k_1}} \qquad [54]$$

then by virtue of [53], $y_0+\mu < 0$. But $y_0-\mu < 0$ so if [54] holds then $\beta_0 \equiv (y_0-\mu)/(y_0+\mu) > 0$. In fact, as $y_0 < 0$, $\beta_0 = (|y_0| + \mu) / (|y_0| - \mu)$ so that $|y_0| > \mu$, in which case $\beta_0 > 1$. Adding [54] to our list of basic assumptions, we have shown that if $y^2(t) > \mu^2$, for $t \geq 0$, then $y(t)$ is given by [50] with $\beta_0 > 0$. From [50], we compute that

$$\dot{y}(t) = 4\mu\beta_0 e^{2\mu At}/(1 - \beta_0 e^{2\mu At})^2 \qquad [55]$$

But, by virtue of [54], $\beta_0 > 1$ so $1 - \beta_0 e^{2\mu At} \neq 0$, for $t > 0$. Using [50] and [55], it is a straightforward exercise to verify that $y(t)$ satisfies [44], and thus, for $y(t)$ as given by [50]

$$y^2(t) - \mu^2 \equiv \frac{\dot{y}(t)}{A} > 0, \text{ for all } t > 0 \qquad [56]$$

By the local uniqueness of solutions to the initial-value problem [45], it now follows that the validity of the solution given by [50] is, in fact, independent of our original assumption that $y^2 > \mu^2$ for $t > 0$.

As $y(t)$, given by [50] satisfies $y^2 > \mu^2$, for $t \geq 0$, we have, by the definitions of $y(t)$ and μ, that

$$n_p^f(t)\left[\frac{n_p^f(t)}{n_p} - \frac{B}{A}\right] > \frac{k_2}{k_1}, \; t > 0 \qquad [57]$$

Using the definitions of A, B, and α, and the fact that $n_p^f(t) = \alpha + n_B^f(t)$, it follows from [57] that

$$n_B^f(t) > \left(\frac{k_2}{k_1}\right)\left(\frac{n_p^a(t)}{n_p^f(t)}\right),\ t > 0 \qquad [58]$$

i.e., the ratio, at time t, of the number of free particles in $\mathcal{V}_f$ to the number of attached particles in $\mathcal{V}_f$ is greater than k_2/k_1 times the inverse of the number of free bubbles in $\mathcal{V}_f$ at time t. As $n_B^f(t) < n_B$ in $\mathcal{V}_f$, at any $t \geq 0$, we also can obtain from [58] the lower bound

$$n_p^f(t)/n_p^a(t) > (k_2/k_1)\,\frac{1}{n_B}$$

which, because $n_p > n_p^f(t)$, at any $t \geq 0$ in $\mathcal{V}_f$, implies that

$$n_p^a(t) < \left(\frac{k_2}{k_1}\right) n_p n_B,\ t \geq 0 \qquad [59]$$

In terms of $\gamma(t)$, the solution [50] assumes the form

$$\gamma(t) = \mu\left[\frac{1 + \beta_0^{-1}e^{-2\mu A t}}{1 - \beta_0^{-1}e^{-2\mu A t}}\right] - \frac{|B|}{2A} \qquad [60]$$

From [60], and the definitions of A, B, μ, and $\gamma(t)$, it follows that

$$\lim_{t\to\infty}\frac{n_p^f(t)}{n_p} = \sqrt{\frac{\left([n_p - n_B]\,k_1 - k_2\right)^2}{4n_p^2k_1^2} + \frac{k_2}{n_p k_1}} - \frac{(k_2 + [n_B - n_p]\,k_1)}{2n_p k_1} \qquad [61]$$

However, for $C/A \equiv \dfrac{k_2}{k_1 n_p}$ small, which is the expected situation, the mean-value theorem yields

$$\mu - \frac{|B|}{2A} \equiv \sqrt{\frac{B^2}{4A^2} + \frac{C}{A}} - \frac{|B|}{2A} \simeq \left(\frac{C}{A}\right)\left(\frac{1}{2\sqrt{x}}\right)\Bigg|_{x=} \frac{B^2}{4A^2}$$

or

$$\mu - \frac{|B|}{2A} \simeq \frac{C}{|B|} \qquad [62]$$

Using [62] in [61], it follows that

$$\lim_{t\to\infty} \frac{n_p^f(t)}{n_p} \simeq \frac{k_2}{k_2 + (n_B - n_p)k_1}, \qquad [63]$$

so that the asymptotic limit of the number of free particles in $\mathcal{V}_f$ is independent of the initial number of free particles in $\mathcal{V}_f$. From [60] and the fact that both β_0 and A are positive, we have

$$\dot{\gamma}(t) = -4\mu^2 A\beta_0 e^{2\mu At}/(\beta_0 e^{2\mu At} - 1)^2 < 0 \qquad [64]$$

while

$$\ddot{\gamma}(t) = 8\mu^3 A^2 \beta_0 e^{2\mu At}\left[\frac{\beta_0 e^{2\mu At} + 1}{(\beta_0 e^{2\mu At} - 1)^3}\right] > 0 \qquad [65]$$

as $\beta_0 > 0$. Thus, the graph of $\gamma(t) = n_p^f(t)/n_p$ is convex and monotonically strictly decreasing, for $t > 0$, with initial slope

$$\dot{\gamma}(0) = -4\mu^2 A\beta_0/(\beta_0 - 1)^2 < 0 \qquad [66]$$

Using our earlier results, it is not difficult to obtain, e.g., an algebraic expression for the initial rate of decrease of the number of free ink particles in $\mathcal{V}_f$ in terms of the basic physical and geometrical parameters that are associated with the flotation cell.

RESULTS AND DISCUSSION

Using the information given by [50] and [64]-[66], the graph of $\gamma(t)$ that is depicted in Fig. 10 is easily obtained. On the graph, $\gamma_\infty = n_{p,\infty}^f/n_p$ where $n_{p,\infty}^f = \lim_{t\to\infty} n_p^f(t)$, $\bar{\gamma}(t)$ is the graph of the tangent line to $\gamma(t)$ at $t = 0$, i.e.,

$$\bar{\gamma}(t) = -\frac{4\mu^2 A\beta_0}{(\beta_0 - 1)^2}t + \frac{n_p^f(0)}{n_p} \qquad [67]$$

$\bar{t}$ is the time at which the graph of $\bar{\gamma}(t)$ intersects the asymptote $\gamma = \gamma_\infty$, i.e.,

$$\bar{t} = \frac{\left(\frac{n_p^f(0)}{n_p}\right) - \gamma_\infty}{4\mu^2 A\beta_0}(\beta_0 - 1)^2, \qquad [68]$$

t^* represents the time required for the ratio of the number of fee ink particles to the total number of ink particles in $\mathcal{V}_f$ to fall to a specified level $\gamma_*, \gamma_\infty < \gamma_* < \frac{n_p^f(0)}{n_p}$, i.e.,

$$t^* = \frac{1}{2\mu A} ln\left[\frac{1}{\beta_0}\left\{\frac{\frac{1}{\mu}\left(\gamma_* + \frac{|B|}{2A}\right) + 1}{\frac{1}{\mu}\left(\gamma_* + \frac{|B|}{2A}\right) - 1}\right\}\right] \qquad [69]$$

and $\hat{\gamma}$ is the level to which the ratio n_p^f/n_p falls in a given time $\hat{t}$.

Referring to the graph of $\gamma(t)$, we note various quantities that can be used to characterize the effectiveness of the flotation deinking process as it applies to the removal of (ink) particles in the volume element $\mathcal{V}_f$. Because the greatest slope on the graph of $\gamma(t)$ occurs at $t = 0$, we could characterize the effectiveness of the process by looking at

$$\mathcal{F}_e^0 = |\dot{\gamma}(0)|/\gamma(0) \qquad [70]$$

and seeking to determine which set of conditions in the cell can be manipulated so as to maximize the initial (relative) rate of decrease of the number of free ink particles in $\mathcal{V}_f$. Using [66] and the definitions of A, μ, and β_0, it can be shown that with $x = n_p^f(0)$

$$\mathcal{F}_e^0(x) = k_1 x + [(n_B - n_p)k_1 + k_2] - \frac{k_2 n_p}{x}, \qquad [71]$$

so that $\mathcal{F}_e^{0'}(x) = k_1 + k_2 n_p / x^2 > 0$; thus, the relative initial ratio $|\dot{\gamma}|/\gamma(0)$ is strictly increasing as the number of initially free ink particles in $\mathcal{V}_f$ increases (for fixed values of n_p, n_B, k_1, and k_2). A more interesting exercise would consist of fixing n_p, n_B, and $n_p^f(0)$ and studying how the expression for $\mathcal{F}_e^0$ varies as one perturbs one or more of the basic physical and/or geometrical parameters which enter into the structure of the kinetic constants k_1, k_2, e.g., one could fix, in the individual probabilities which govern the microprocesses, all parameters such as R_p, R_b, v_B, σ, etc., and vary only the measure ϵ of the turbulent flow field in the flotation cell so as to obtain $\mathcal{F}_e^0 = \mathcal{F}_e^0(\epsilon)$.

One measure of the efficiency of the deinking process that is naturally suggested by the graph of $\gamma(t)$ is

$$\mathcal{F}_e^\infty \equiv 1 - \frac{n_{p,\infty}^f}{n_p^f(0)} \simeq 1 - \left(\frac{n_p}{n_p^f(0)}\right) \frac{k_2}{k_2 + (n_B - n_p)k_1} \qquad [72]$$

From (72) and the fact that $n_{p,\infty}^f < n_p^f(0)$, irrespective of the value of $n_p^f(0)$, we have $0 < \mathcal{F}_e^\infty < 1$, with $\mathcal{F}_e^\infty \to 1$ as $k_2 \to 0$. Clearly, $\mathcal{F}_e^\infty$ may be expressed in terms of the basic geometrical and physical parameters of the flotation deinking cell such as R_p, R_B, σ, v_B, etc., and it will be of interest, in future work, to carefully study the dependence of $\mathcal{F}_e^\infty$ on variations in these parameters.

Two other measures of the effectiveness of the flotation deinking model are connected with the definitions of the points (t^*, γ_*) and $(\hat{t}, \hat{\gamma})$ on the graph of $\gamma(t)$. Recall that t^*, as

given by [69], represents the time required for the ratio of the number of free ink particles in $\mathcal{V}_f$ to the total number of particles in $\mathcal{V}_f$ to fall to a specified level $\gamma_*, \gamma_\infty < \gamma_* < \frac{n_p^f(0)}{n_p}$. If, for example, one were to specify that $\gamma_* = \frac{1}{2}\frac{n_p^f(0)}{n_p}$, then [69] yields

$$t_{1/2} \simeq \frac{1}{2\mu A} ln \left[\frac{1}{\beta_0} \left\{ \frac{\frac{1}{\mu}\left(\frac{1}{2}\frac{n_p^f(0)}{n_p} + \frac{|B|}{2A}\right) + 1}{\frac{1}{\mu}\left(\frac{1}{2}\frac{n_p^f(0)}{n_p} + \frac{|B|}{2A}\right) - 1} \right\} \right] \qquad [73]$$

By substituting for β_0, μ, and $\frac{|B|}{2A}$ in [73], in terms of n_p, n_B, k_1, k_2, and then for the rate constants k_1 and k_2 in terms of the basic physical and geometrical parameters in the flotation cell, one could study how $t_{1/2}$ depends on R_p, R_B, v_B, etc., and seek to minimize $t_{1/2}$ as a function of one or more of these controllable parameters. Finally, we may avail ourselves of the interpretation of the point $(\hat{t}, \hat{\gamma})$ on the graph of $\gamma(t)$ in Fig. 10, i.e., for a given $\hat{t}, \hat{\gamma}$ is the level to which $\gamma(t)$ falls in time $\hat{t}$. This leads, of course, to the result

$$\hat{\gamma} = \mu \left[\frac{1 + \beta_0^{-1} e^{-2\mu A \hat{t}}}{1 - \beta_0^{-1} e^{-2\mu A \hat{t}}} \right] - \frac{|B|}{2A} \qquad [74]$$

and the right-hand side of [74] can also be expressed in terms of all the basic geometrical and physical parameters associated with the cell. Since, for a given fixed time $\hat{t} > 0$, it is desirable to have the ratio $\hat{\gamma} \equiv n_p^f(\hat{t})/n_p$ as low as possible, it would be an important exercise to study the variation of $\hat{\gamma}$, for fixed $\hat{t}, n_p, n_B$, and $n_p^f(0)$, as a function of one or more of the basic physical and/or geometrical parameters, with the goal of minimizing $\hat{\gamma}$; such considerations are now the subject matter of ongoing research efforts.

Predictions of flotation performance can be obtained by employing [67] and selecting appropriate physical parameters (i.e., $R_B, R_p, v_B, \rho_p, \rho_\ell, \epsilon, \sigma$, etc.). Following Schulze (23), we utilize $d_B = (\sigma/\rho_\ell)^{0.6}/\epsilon^{0.4}$ to eliminate surface tension (σ) from the required physical

parameters. We also assume v_B = constant = 10 cm/s for these calculations as an initial approximation and that the liquid properties correspond to those of water. The remaining system parameters ($R_B, R_p, \rho_p, \epsilon, \theta, \phi^*_{crit}, n_B, n_p$) are chosen based on experimental and theoretical parametric ranges utilized by other investigators for flotation studies with standard conditions referring to fixed values. Finally, we employ the Liepe-Möckel correlation for the collision frequency (22), and assume that, at time $t = 0$, all particles are free and unattached to bubbles in the unit volume (i.e., $n_p^f(0) = n_p$).

Figure 11 reveals the predicted flotation efficiency as a function of flotation time for five selected particle radii, while all other parameters are held constant at their standard conditions (i.e., $R_B = 0.5\ mm$, $\rho_p = 1.3\ g/cm^3$, $\epsilon = 10\ W/kg$, $\theta = 60°$, $\phi^*_{crit} = 60°$, $n_B = 1000$, and $n_p = 100$). For $R_p \lesssim 50\ \mu m$, the flotation efficiency asymptotes to 1.0. However, in actual flotation deinking operations, small particles of $R_p \lesssim 10\ \mu m$ are not effectively removed because, as shown in Fig. 11, these particles require a long time period to reach an efficiency of 1.0. For example, for $R_p = 1\ \mu m$, a flotation time of more than 1 hour in a unit volume is required to effectively remove these particles, whereas flotation time (stock residency time) in a typical flotation cell is approximately 10 to 15 minutes and the residence time in a typical unit volume is on the order of 1-2 seconds. Increasing the particle radius results in a reduction in time required to reach a constant flotation efficiency. For particles with $R_p = 100\ \mu m$ and $R_p = 200\ \mu m$, the efficiency asymptotes to constant values $\mathcal{F}_e^\infty \simeq 0.99$ and $\mathcal{F}_e^\infty \simeq 0.97$, respectively. Calculations for larger particle radii, at the given fixed conditions, result in predictions where $P_{stab} < 0$, indicating these aggregates are unstable for the given conditions, and are not shown in the figure. The interaction between bubble radius, R_B, and particle radius, R_p, and their effect on flotation efficiency can be identified by utilizing [72] and focusing on flotation efficiency predictions for an infinite

time period. However, one must be cognizant of the fact that an infinite time period for $R_p = 1\ \mu m$ is on the order of hours, while for $R_p = 100\ \mu m$, it is on the order of tenths of seconds. Figure 12 displays this relationship over the entire range of particle radii for selected bubble radii and fixed values of $\rho_p = 1.3\ g/cm^3, \epsilon = 10\ W/kg, \theta = 60°$, $\phi^*_{crit} = 60°$, $n_B = 1000$, and $n_p = 100$. As highlighted in Fig. 11 and displayed in Fig. 12, particles with small radii ($R_p \lesssim 10\ \mu m$) will asymptote to a flotation efficiency of 1.0 for all bubble radii considered, but this time may well surpass typical residence times in a unit volume. For $R_B = 0.1\ mm$, the efficiency drops rapidly when $R_p > 10\ \mu m$. Similar patterns are observed at larger bubble radii, but the rapid decline in efficiency occurs at larger particle radii as the bubble radius increases; this is the expected result because particles of a given size can only be removed if bubbles are large enough to overcome all destabilizing forces on the particle/bubble aggregate. Finally, for the given fixed parameters, specific particle-bubble radii combinations result in unrealistic predictions due to model limitations, and these data are omitted from the figure.

Figure 13 displays the effect particle radius has on flotation efficiency at infinite flotation time for selected turbulent energy densities, while the remaining parameters are held constant at $R_B = 0.5\ mm$, $\rho_p = 1.3\ g/cm^3$, $\theta = 60°$, $\phi^*_{crit} = 60°, n_B = 1000$, and $n_p = 100$. All particles less than $R_p = 60\ \mu m$ are predicted to be removed given enough time in a unit volume. Efficiency begins to rapidly decline when $R_p \gtrsim 60\ \mu m$, occurring first when $\epsilon = 1\ W/kg$; as the particle radius increases, this trend is eventually observed when $\epsilon = 400\ W/kg$. It appears that for the given fixed conditions, the turbulent energy density is more important in bringing particles in contact with bubbles (the collision frequency) than in destabilizing the particle/bubble aggregate because the larger ϵ is, the higher the collision frequency [39] and detaching force [30], which increases and decreases flotation

efficiency, respectively. However, eventually the destabilizing forces are more significant and the flotation efficiency at infinite time drops significantly. For the given conditions, no particles with $R_p \gtrsim 250\ \mu m$ will be removed because all predicted efficiencies drastically decline at this particle radius. It is reasonable to assume that similar families of curves can be generated using these selected values of ϵ over the entire range of particle radii, but at other fixed bubble radii (i.e., $R_B = 0.1, 0.3, 1.0\ mm$, etc.), the maximum particle radius removed would be more sensitive to bubble radius (Fig. 12) than turbulent energy density (Fig. 13).

Additional predictions, based on other flotation performance parameters, are currently under study and will be the subject of a future report.

SUMMARY AND CONCLUSIONS

A kinetic- or population balance-type model has been developed, utilizing the various microprocesses associated with flotation, to model the overall flotation deinking process. The overall model contains two kinetic constants: the first, k_1, governs the overall probability that a free particle will successfully intercept and adhere to an air bubble; the second, k_2, describes the probability that a particle/bubble aggregate will become unstable and separate to yield a "new" free particle in the system. These kinetic constants were presented in terms of the individual microprocess probabilities, which are themselves functions of system parameters.

The solution to the kinetic equation has been presented in terms of the kinetic constants from which a theoretical flotation efficiency has been defined. Additional system performance parameters have also been presented in terms of the kinetic constants, which provide supplemental measures of flotation system performance.

Various assumptions were incorporated into the model to yield a solution to the governing equation. Relaxation of these assumptions is the goal of future research.

ACKNOWLEDGEMENT

The work described in this paper was funded by the Member Companies of the Institute of Paper Science and Technology. Their continued support is gratefully acknowledged.

REFERENCES

1. McCool, M.A., *in* "Secondary Fiber Recycling," (R.J. Spangenberg, Ed.), p. 141. TAPPI Press, Atlanta, GA, 1993.

2. Ferguson, L.D., *in* "1995 Deinking Short Course Notes," Chapter 10. TAPPI Press, Atlanta, GA, 1995.

3. Woodburn, E.T., *Minerals. Sci. Engng.* **2,** 3(1970).

4. Schulze, H.J. "Physico-chemical Elementary Processes in Flotation." Elsevier Pub., Amsterdam, 1984.

5. Pan, R., Bousfield, D., and Thompson, E., *in* "1992 TAPPI Pulping Conference Proceedings," p.941. TAPPI Press, Atlanta, GA, 1992.

6. Bilsing, U., *Freiberger Forschungsh* **A368**, 7 (1981).

7. Plate, H., and Schulze, H.J. *in* "XVII Internat. Mineral Processing Congress," Dresden, Sept. 23-28, p.365. 1991.

8. Schulze, H.J., *in* "Coagulation and Flocculation" (B. Dobias, Ed.), p. 321. 1993.

9. Schulze, H.J., *in* "1991 TAPPI Recycling Forum Proceedings," p.161. TAPPI Press, Atlanta, GA, 1991.

10. Schulze, H.J. *Advances in Colloid and Interface Science* **40,** 283 (1992).

11. Yoon, R.H., and Luttrell, G.H., *Mineral Processing and Extractive Metallurgy Review* **5**, 101 (1989).

12. Dukhin, S.S., Rulev, N.N., and Dimitrov, A.S., "Koagulyastsiya i Dinamika Tonkikh." Naukova Dumka, Kiev, 1986.

13. Derjaguin, B.V., Dukhin, S.S., and Rulev, N.N., "Microflotacija." Chimija Moskva, 1986.

14. Ahmed, N., and Jameson, G.J., *in* "Frothing in Flotation," (J. Laskowski, Ed.), p. 77. Gordon and Breach, New York, 1989.

15. Derjaguin, B.V. Dukhin, S.S., and Rulev, N.N., *Colloid Journal of the USSR* **39,** Part 1, 926 (1977).

16. Williams, M., and Davis, S.H., *J. Colloid and Interface Science* **90,** 220 (1982).

17. Paulsen, F.G., Pan, R., Bousfield, D., and Thompson, E., *in* "2nd Research Forum on Recycling," p. 1. TAPPI Press, Atlanta, GA, 1993.

18. Plate, H., Ph.D. thesis, ADW, UVR Freiberg/Sa. Chemnitzer Str. 40, unpubl. (work quoted in Schulze (8)).

19. Sutherland, K.L., *J. Phys. Chem.* **51**, 394 (1948).

20. Saffman, P.G., and Turner, T.S., *Fluid Mech.*, **1**, 16 (1956).

21. Camp, T.R., and Stein, P.C., *J. Boston Soc. Civil Engrs.* **30,** 219 (1943).

22. Liepe, F., and Möckel, O.H., *Chem. Techn.* **28,** 205 (1976).

23. Schulze, H.J. *Wochenblatt für Papierfabrikation* **122**, 160 (1994).

Appendix: The Thin-Film Equations

In this paper, two forms of the equation that governs the thickness of the thin film separating a particle from a bubble have been introduced, i.e., [14], [15], which is taken from the work of Derjaguin et al. (15), as reported in Schulze (4), and [18], which is taken from the work of Williams and Davis (16). In this Appendix we will indicate how [14], [15], and [18] may be viewed as different coordinate realizations of the same coordinate invariant equation

$$\frac{\partial h}{\partial t} = \frac{\sigma}{3\mu_\ell} \bigtriangledown \cdot [h^3 \bigtriangledown \left(\bigtriangledown^2 h \right)] \qquad \text{[A1]}$$

when one uses the capillary pressure

$$P_\sigma = \sigma \bigtriangledown^2 h \qquad \text{[A2]}$$

employs the appropriate interpretation of h, and uses mathematical assumptions which correctly reflect the particular nature of the physical problem at hand.

Consider, first of all, [18]; we claim that this equation is identical with [A1]; when the disjoining pressure is just given by the capillary pressure [A2], we employ the polar coordinate system (r, θ) on the bubble surface S_B, which is indicated in Fig. 14a, and we take $x = R_B \theta$. If h is the distance from the particle surface to the bubble surface (as measured along the radial line joining the centers of the particle and the bubble), then

$$\bigtriangledown^2 h \equiv \frac{1}{r^2} \frac{\partial^2 h}{\partial \theta^2} \qquad \text{[A3]}$$

as $h = h(\theta)$. However, with $x = R_B \theta$,

$$\begin{cases} \left. \dfrac{\partial h}{\partial \theta} \right|_{S_B} = \dfrac{\partial h}{\partial x} \dfrac{\partial x}{\partial \theta} \equiv R_B \dfrac{\partial h}{\partial x} \\ \left. \dfrac{\partial^2 h}{\partial \theta^2} \right|_{S_B} = \dfrac{\partial}{\partial x} \left(R_B \dfrac{\partial h}{\partial x} \right) \dfrac{\partial x}{\partial \theta} \equiv R_B^2 \dfrac{\partial^2 h}{\partial x^2} \end{cases}$$

so that

$$\nabla^2 h\big|_{S_B} = \frac{1}{R_B^2}\frac{\partial^2 h}{\partial \theta^2}\bigg|_{S_B} \equiv \frac{\partial^2 h}{\partial x^2} \qquad [A4]$$

Thus,

$$P_\sigma|_{S_B} = \sigma \frac{\partial^2 h}{\partial x^2} \qquad [A5]$$

Also,

$$\left(\nabla|_{S_B}\right) = \left(\frac{\partial}{\partial r}, \frac{1}{r}\frac{\partial}{\partial \theta}\right)\bigg|_{r=R_B} \equiv \left(0, \frac{\partial}{\partial x}\right) \qquad [A6]$$

so that

$$\nabla P_\sigma|_{S_B} = \left(0, \frac{\partial}{\partial x}P_\sigma\bigg|_{S_B}\right) = \left(0, \sigma\frac{\partial^3 h}{\partial x^3}\right) \qquad [A7]$$

Finally,

$$\begin{aligned} \nabla \cdot \left(h^3 \nabla P_\sigma|_{S_B}\right) &= \nabla \cdot \left(0, \sigma h^3 \frac{\partial h}{\partial x^3}\right) \\ &= \left(\frac{1}{r}\frac{\partial}{\partial r}r, \frac{1}{r}\frac{\partial}{\partial \theta}\right)\bigg|_{S_B} \cdot \left(0, \sigma h^3 \frac{\partial^3 h}{\partial x^3}\right) \\ &= \sigma \frac{\partial}{\partial x}\left(h^3 \left(\frac{\partial P_\sigma}{\partial x}\right)\bigg|_{S_b}\right) \end{aligned} \qquad [A8]$$

or

$$\nabla \cdot \left(h^3 \nabla P_\sigma\big|_{S_B}\right) \equiv \frac{\partial}{\partial x}\left(h^3 \left(\frac{\partial P_\sigma}{\partial x}\right)\bigg|_{S_B}\right) \qquad [A9]$$

as $\sigma\dfrac{\partial^3 h}{\partial x^3} = \dfrac{\partial}{\partial x}P_\sigma\bigg|_{S_B}$, by virtue of [A6] and [A7]. From [A9], it follows directly that [18] is equivalent to [A1], [A2], in the chosen coordinate system on S_B, with $x = R_B\theta$. For the derivation of [14], [15] from [A1], we use the local cylindrical coordinate system shown in Fig. 14b; in this case, it is assumed that the spherical particle is approaching the bubble surface normal to that surface. The coordinate x in [14], [15] will coincide with the local radial coordinate in Fig. 14b. The total distance between the particle surface and the deformed bubble surface is given by

$$h(x,t) \equiv h(r,t) = h_1(x,t) + \hat{h}(t) + \frac{x^2}{2R_p} \qquad \text{[A10]}$$

where h_1 is the distance between the deformed bubble surface and the (originally) undeformed bubble surface at (x,t); $\hat{h}(t)$ is the distance, at time t, between the particle surface and the undeformed bubble surface at $x = 0$; and $x^2/2R_p$ is the distance, at radial coordinate value x, between the particle surface and the tangent line to the particle surface through the point on that surface which corresponds to $x = 0$. We have

$$\frac{\partial \hat{h}}{\partial t} = v_p \qquad \text{[A11]}$$

where v_p is the velocity of approach of the particle to the bubble surface as measured along the radial line joining the centers of the particle and the bubble. On the left-hand side of [A1], therefore,

$$\frac{\partial h}{\partial t} = \frac{\partial h_1}{\partial t} + v_p \simeq v_p \qquad \text{[A12]}$$

as it is assumed in [15] that $\dfrac{\partial h_1}{\partial t} \simeq 0$. Next, in the coordinate system shown in Fig. 14b, with x the local *radial* coordinate,

$$\nabla^2 h \equiv \frac{1}{x}\frac{\partial}{\partial x}\left(x\frac{\partial h}{\partial x}\right) \qquad \text{[A13]}$$

as $\dfrac{\partial h}{\partial \theta} \equiv 0$. Thus, by comparing [A13] with [13] we see, indeed, that [A2] holds provided R_p^{-1} is small in comparison with $\dfrac{1}{x}\left|\dfrac{\partial h_1}{\partial x}\right|$ and $\left|\dfrac{\partial^2 h_1}{\partial x_1^2}\right|$; indeed, under those circumstances, by [A10]

$$\begin{cases} \dfrac{\partial^2 h}{\partial x^2} = \dfrac{\partial^2 h_1}{\partial x^2} + \dfrac{1}{R_p} \simeq \dfrac{\partial^2 h_1}{\partial x^2} \\ \dfrac{1}{x}\dfrac{\partial h}{\partial x} = \dfrac{1}{x}\dfrac{\partial h_1}{\partial x} + \dfrac{1}{R_p} \simeq \dfrac{1}{x}\dfrac{\partial h_1}{\partial x} \end{cases} \qquad \text{[A14]}$$

Thus, to the degree of approximation associated with [A14], [A13] becomes

$$\nabla^2 h \simeq \nabla^2 h_1 = \frac{1}{x}\frac{\partial}{\partial x}\left(x\frac{\partial h_1}{\partial x}\right) \qquad \text{[A15]}$$

Continuing, we have

$$\begin{aligned} \nabla(\nabla^2 h) &\simeq \nabla(\nabla^2 h_1) \\ &= \left(\frac{\partial}{\partial x}\nabla^2 h_1, \frac{1}{x}\frac{\partial}{\partial \theta}\nabla^2 h_1\right) \\ &= \left(\frac{\partial^3 h_1}{\partial x^3} + \frac{1}{x}\frac{\partial^2 h_1}{\partial x^2} - \frac{1}{x^2}\frac{\partial h_1}{\partial x}, 0\right) \end{aligned} \qquad \text{[A16]}$$

and

$$\begin{aligned} \nabla \cdot [h^3 \nabla (\nabla^2 h)] &\simeq \nabla \cdot [h^3 \nabla (\nabla^2 h_1)] \\ &= \frac{1}{x}\frac{\partial}{\partial x}\left[xh^3\left(\frac{\partial^3 h_1}{\partial x^3} + \frac{1}{x}\frac{\partial^2 h_1}{\partial x^2} - \frac{1}{x^2}\frac{\partial h_1}{\partial x}\right)\right] \end{aligned} \qquad \text{[A17]}$$

By virtue of [A17] and [A12], therefore, [A1] assumes the form

$$\frac{1}{x}\frac{\partial}{\partial x}\left[xh^3\left(\frac{\partial^3 h_1}{\partial x^3} + \frac{1}{x}\frac{\partial^2 h_1}{\partial x^2} - \frac{1}{x^2}\frac{\partial h_1}{\partial x}\right)\right] = \left(\frac{3\mu_\ell}{\sigma}\right) v_p \qquad \text{[A18]}$$

an integration of which yields

$$xh^3\left(\frac{\partial^3 h_1}{\partial x^3} + \frac{1}{x}\frac{\partial^2 h_1}{\partial x^2} - \frac{1}{x^2}\frac{\partial h_1}{\partial x}\right) = \left(\frac{3\mu_\ell v_p}{2\sigma}\right) x^2 + C \qquad \text{[A19]}$$

Setting $x = 0$ in [A19], we see that the constant of integration $C = 0$ so that

$$\frac{\partial^3 h_1}{\partial x^3} + \frac{1}{x}\frac{\partial^2 h_1}{\partial x^2} - \frac{1}{x^2}\frac{\partial h_1}{\partial x} = \left(\frac{3\mu_\ell v_p}{2\sigma}\right)\frac{x}{h^3} \qquad \text{[A20]}$$

which, by virtue of [A10], is the same as [14], [15] if, in the expression [A10] for $h(x,t)$, we follow Derjaguin et al. (15) and replace $h_1(x,t) \simeq h_1(x)$ by $h_1(x,t) \simeq h_1(0)$.

Figure 1: Schematic of the Black Clawson IHI/BC flotation cell. (Reprinted with permission from M.A. McCool, *Secondary Fiber Recycling*, R.J. Spangenberg (ed), p. 150. Copyright ©1993, TAPPI Press.)

Figure 2: A particle intercepting an air bubble at angle ϕ_T.

Figure 3: Forces acting on a particle as it approaches a bubble.

Figure 4: Forces acting on a particle as it slides around a bubble.

Figure 5: Schematic of the thin film formed between the bubble and particle.

Figure 6: Relationship between the touching angle, ϕ_T, and the critical position angle, ϕ^*_{crit}.

Figure 7: The relationship of ϕ^*_{crit} with respect to ϕ_T and h_{crit}.

Figure 8: Three-phase contact between the bubble, particle, and fluid regions.

Figure 9: Forces acting on a bubble/particle aggregate.

Figure 10: Performance parameters identified with the flotation model.

Figure 11: Flotation efficiency as a function of flotation time for selected particle radii, R_p. All other parameters are at standard conditions: $R_B = 0.5\ mm$, $\rho_p = 1.3\ g/cm^3$, $\epsilon = 10\ W/kg$, $\theta = 60°$, ${\phi^*}_{crit} = 60°$, $n_B = 1000$, and $n_p = 100$.

Figure 12: Flotation efficiency at infinite time as a function of particle radius, R_p, for selected bubble radii, R_B. All other parameters are at standard conditions: $\rho_p = 1.3\ g/cm^3$, $\epsilon = 10\ W/kg$, $\theta = 60°$, ${\phi^*}_{crit} = 60°$, $n_B = 1000$, and $n_p = 100$.

Figure 13: Flotation efficiency at infinite time as a function of particle radius, R_p, for selected turbulent energy densities, ϵ. All other parameters are at standard conditions: $R_B = 0.5\ mm$, $\rho_p = 1.3\ g/cm^3$, $\theta = 60°$, ${\phi^*}_{crit} = 60°$, $n_B = 1000$, and $n_p = 100$.

Figure 14: Geometries and coordinate systems associated with the disjoining film dynamics equations.

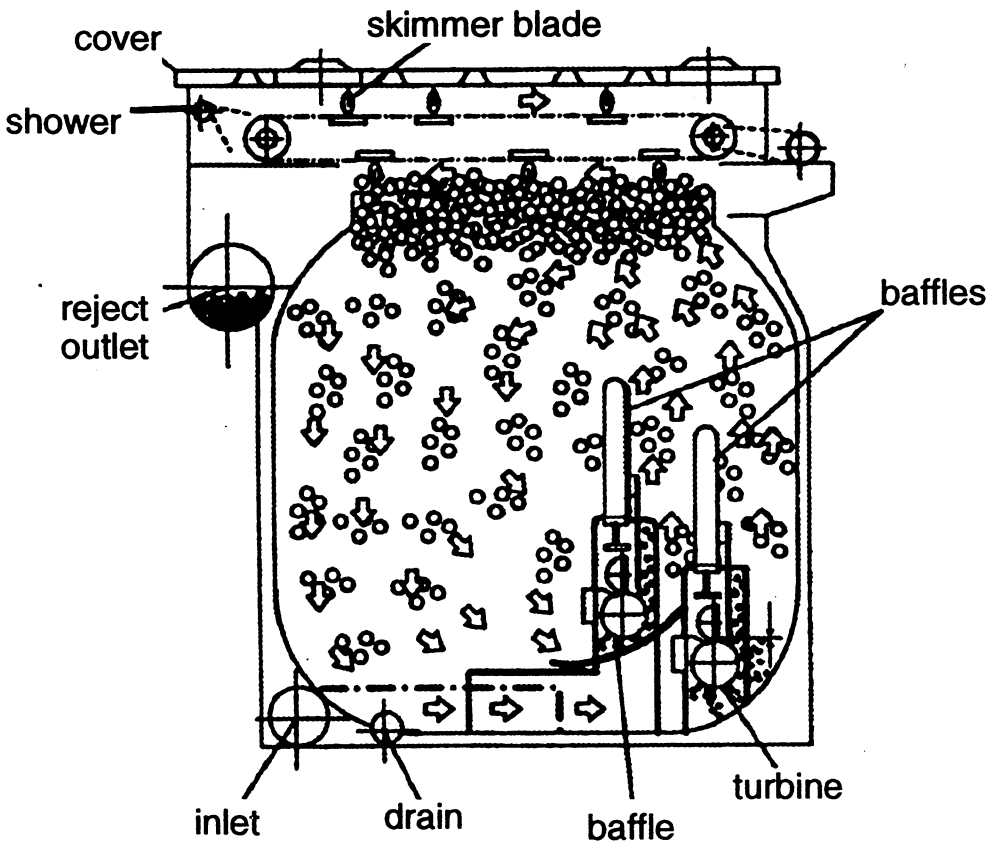
cover
skimmer blade
shower
reject
outlet
baffles
inlet
drain
baffle
turbine

Figure 1

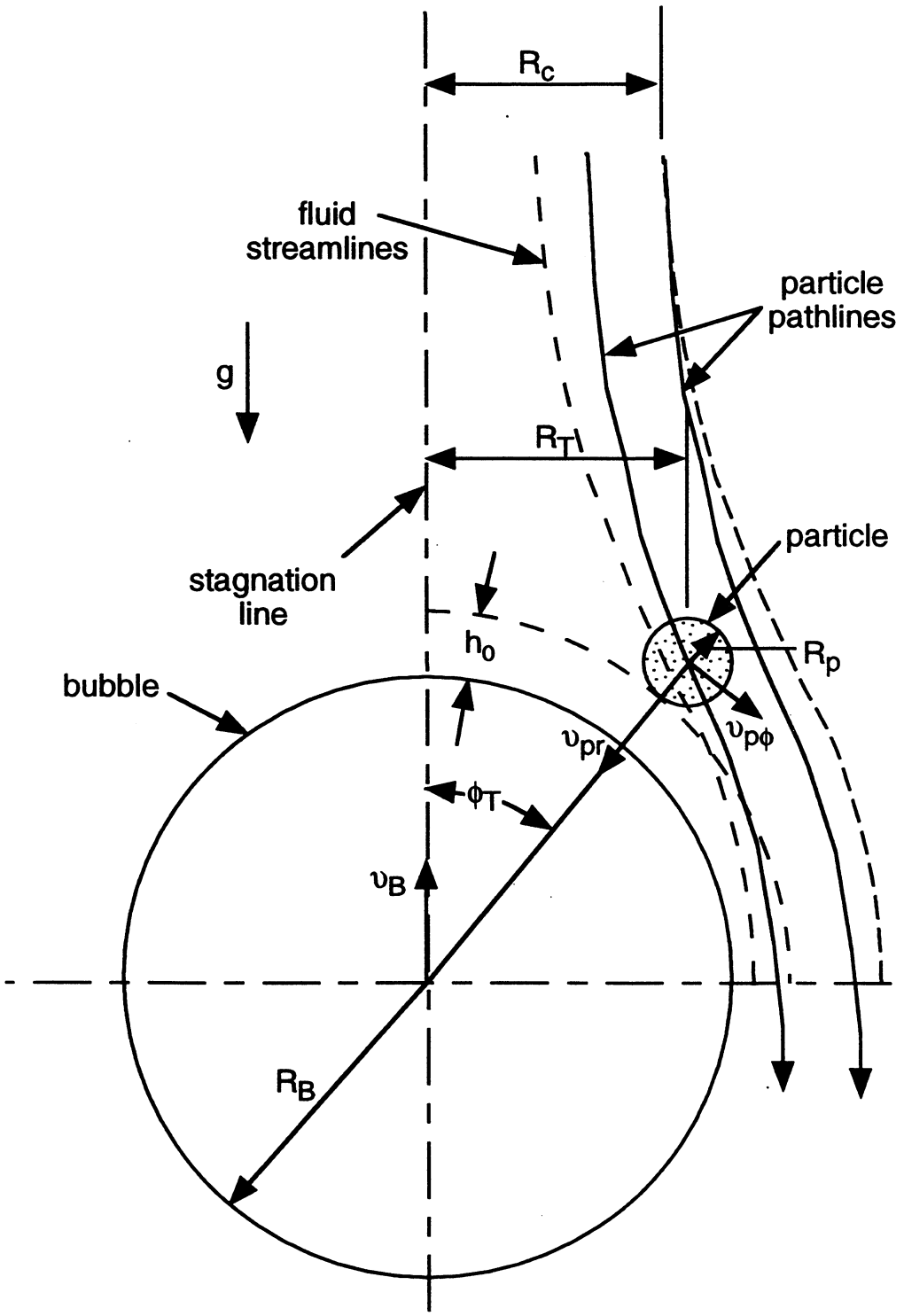
R_c
fluid
streamlines
particle
pathlines
g
R_T
particle
stagnation
line
h_0
R_p
bubble
v_{pr}
$v_{p\phi}$
ϕ_T
v_B
R_B

Figure 2

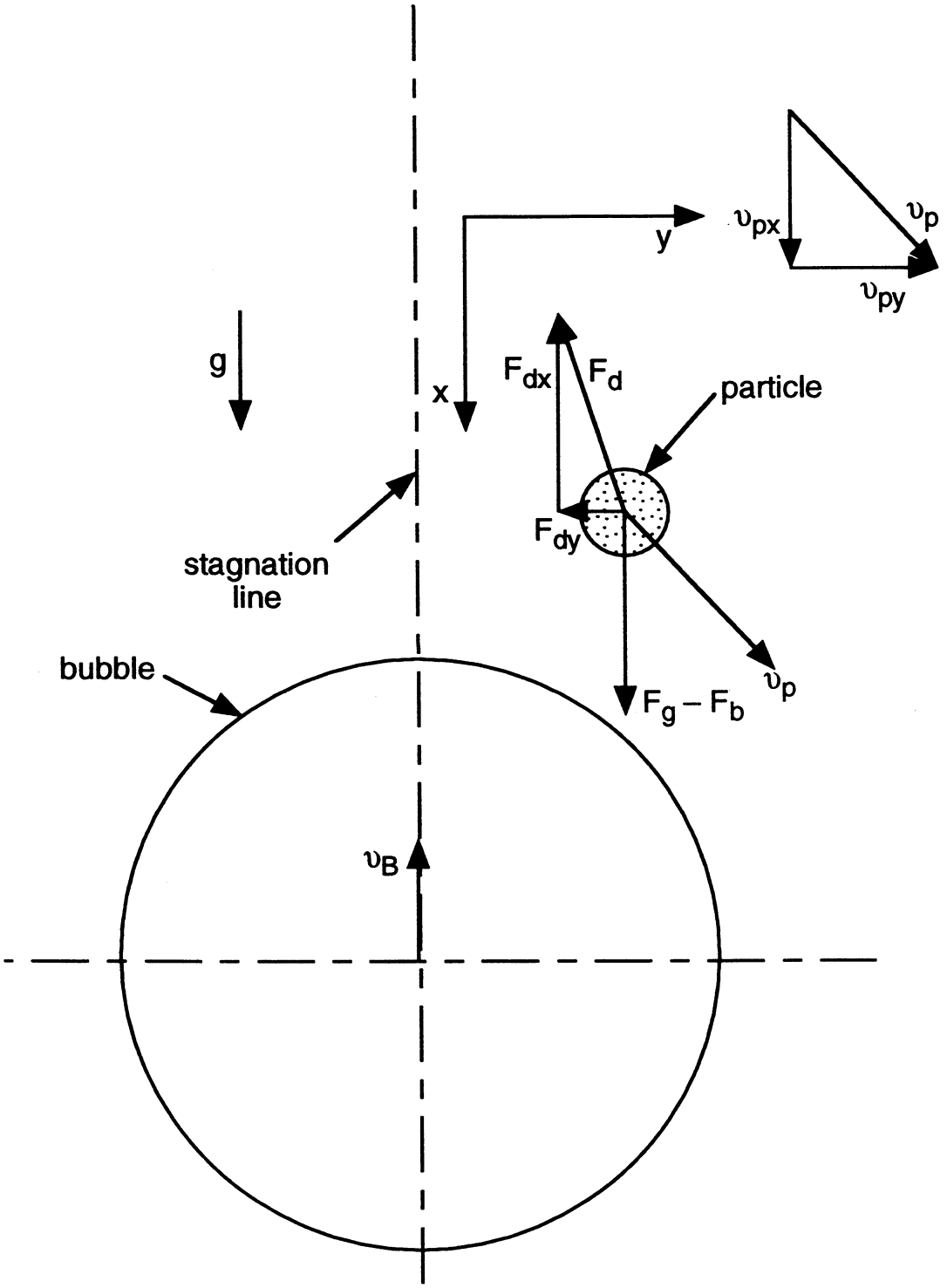
y
υ_{px}
υ_p
υ_{py}
g
x
F_{dx}
F_d
particle
F_{dy}
stagnation
line
bubble
υ_p
$F_g - F_b$
υ_B

Figure 3

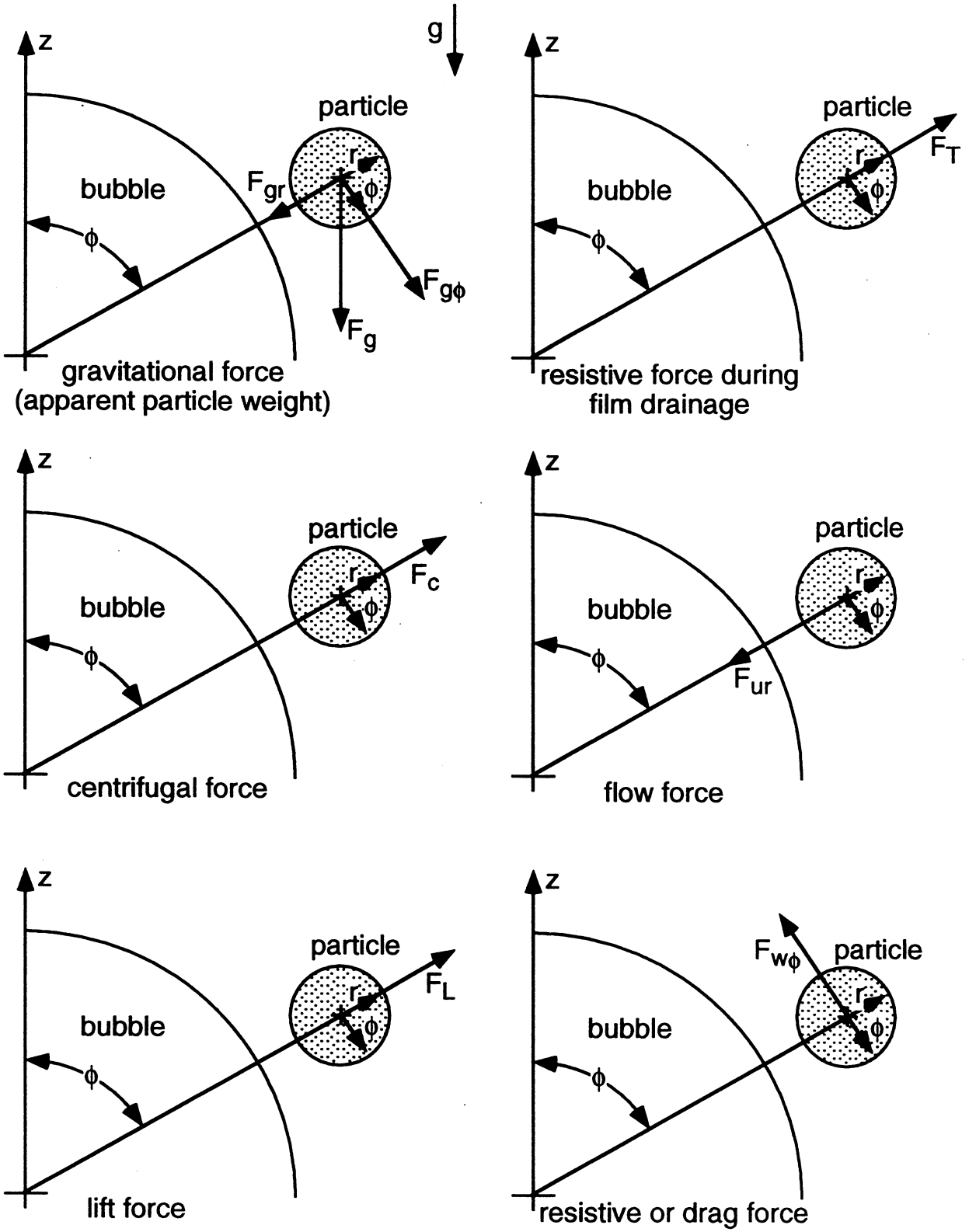
z
g
particle
r
ϕ
bubble
ϕ
F_{gr}
$F_{g\phi}$
F_g
gravitational force
(apparent particle weight)
z
particle
F_T
r
ϕ
bubble
ϕ
resistive force during
film drainage
z
particle
r
ϕ
F_c
bubble
ϕ
centrifugal force
z
particle
r
ϕ
bubble
ϕ
F_{ur}
flow force
z
particle
F_L
r
ϕ
bubble
ϕ
lift force
z
$F_{w\phi}$
particle
r
ϕ
bubble
ϕ
resistive or drag force

Figure 4

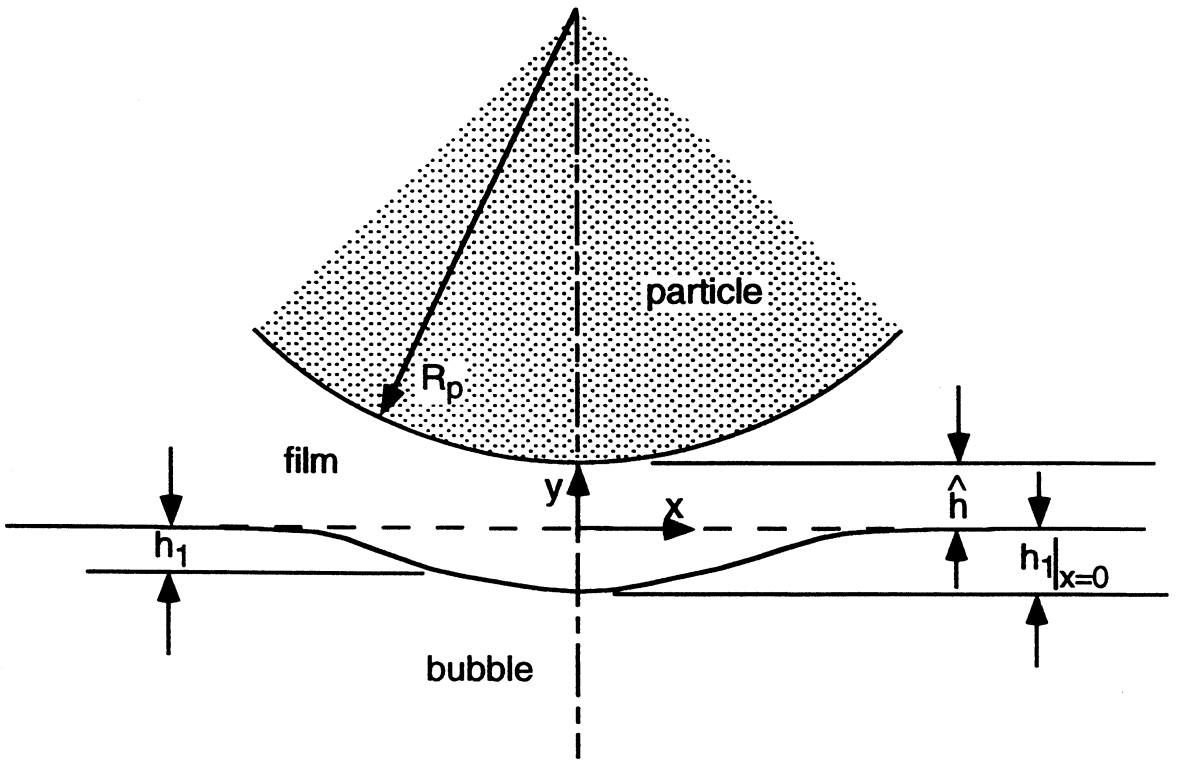

Figure 5

(a) $\phi_T < \phi^*_{crit}$
h_o
ϕ_T
ϕ_{crit}
bubble
h_{crit}
particle path
(b) $\phi_T = \phi^*_{crit}$
h_o
bubble
ϕ_T
$\phi_{crit} < \pi/2$
h_{crit}
particle path
(c) $\phi_T > \phi^*_{crit}$
h_o
bubble
ϕ_T
h_{crit}
particle path
no attachment

Figure 6

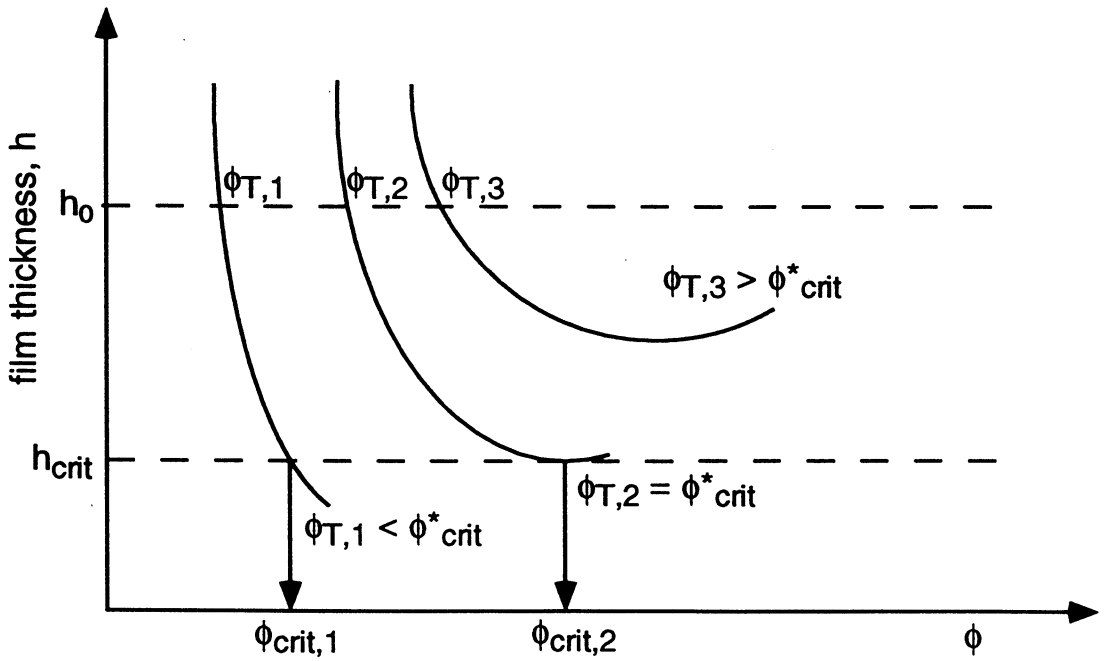
film thickness, h
h_o
h_{crit}
$\phi_{T,1}$
$\phi_{T,2}$
$\phi_{T,3}$
$\phi_{T,3} > \phi^*_{crit}$
$\phi_{T,2} = \phi^*_{crit}$
$\phi_{T,1} < \phi^*_{crit}$
$\phi_{crit,1}$
$\phi_{crit,2}$
ϕ

Figure 7

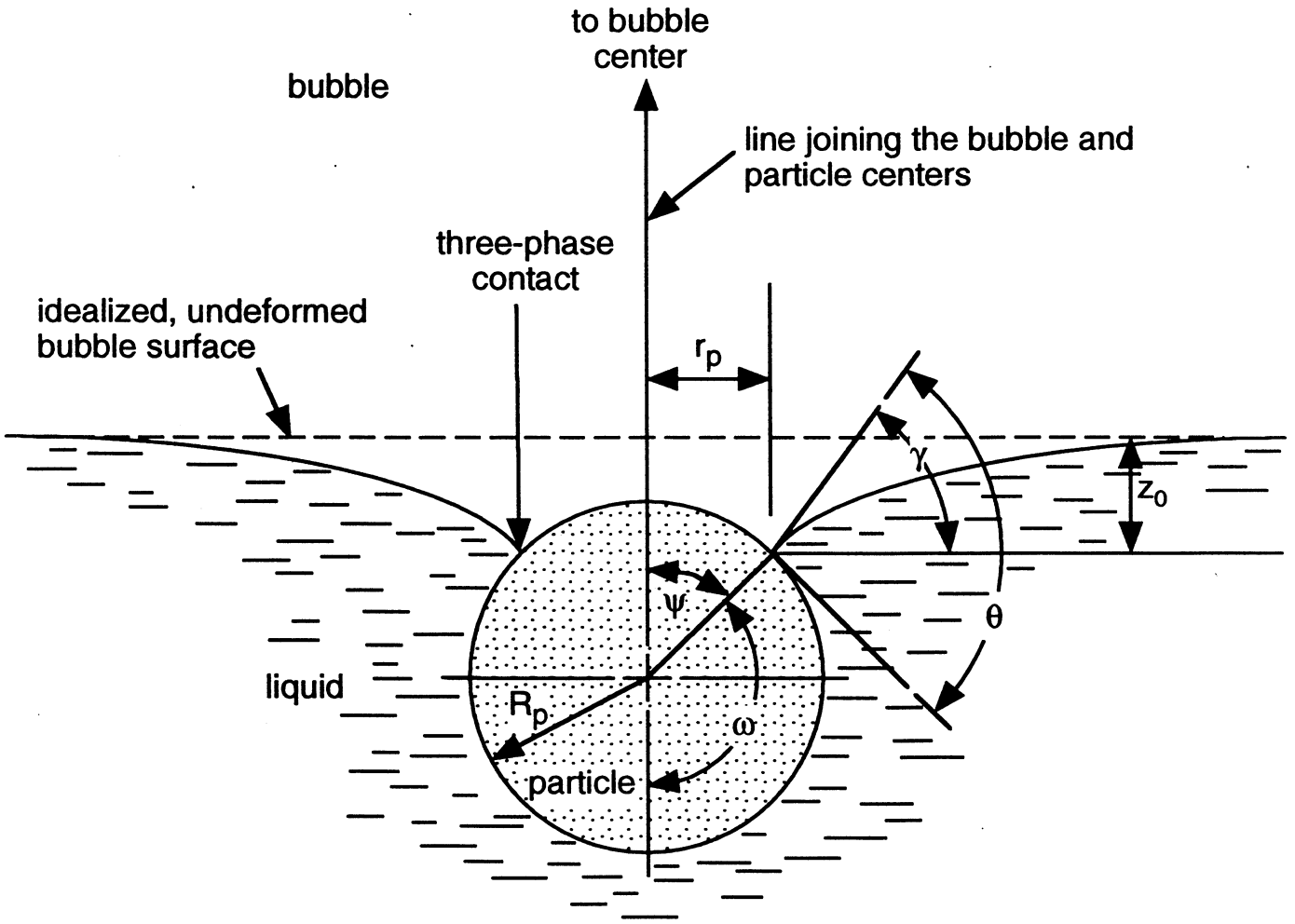
to bubble
center
bubble
line joining the bubble and
particle centers
three-phase
contact
idealized, undeformed
bubble surface
r_p
γ
z_0
ψ
θ
liquid
R_p
ω
particle

Figure 8

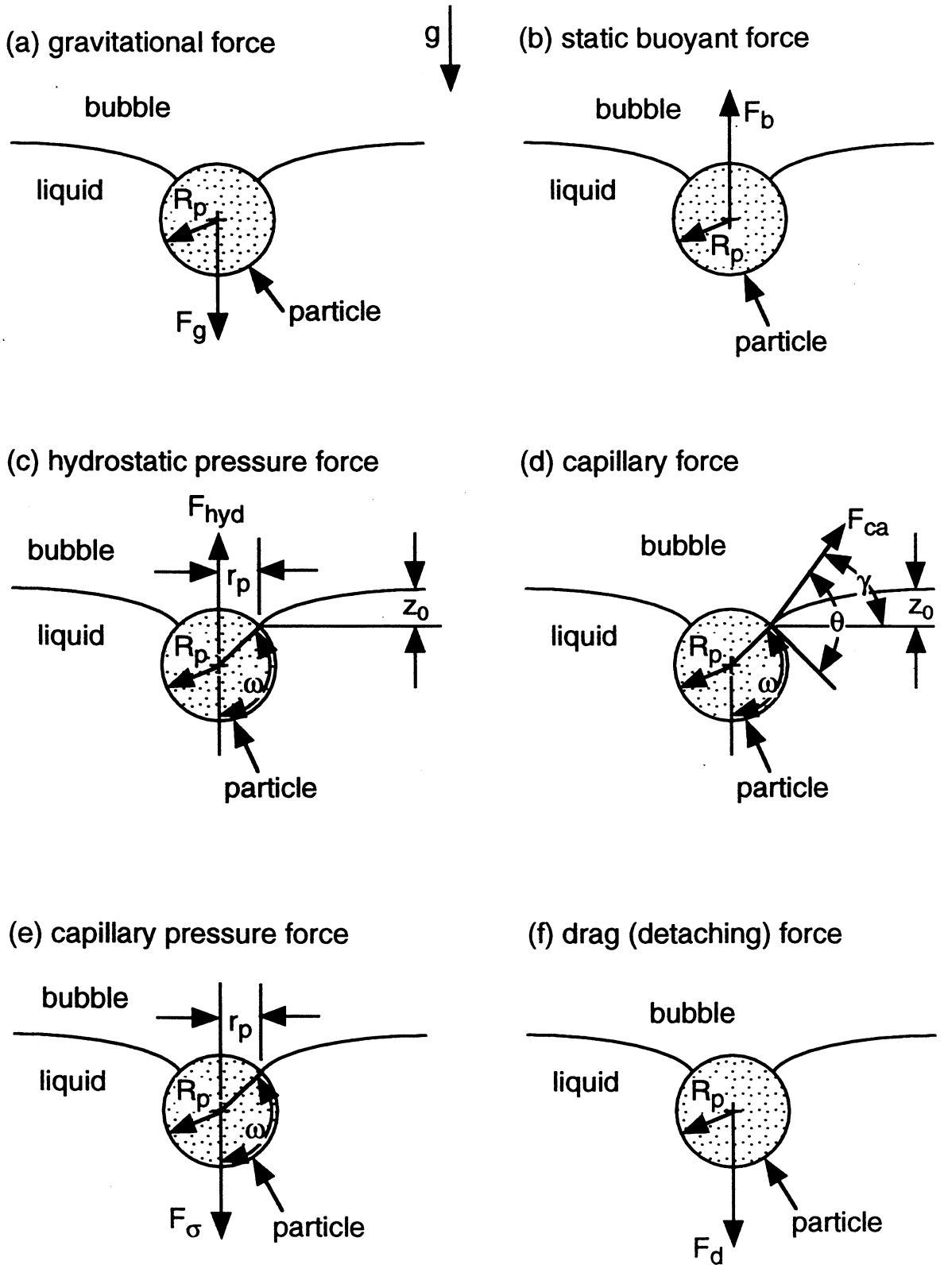
(a) gravitational force
g
bubble
liquid
R_p
F_g
particle
(b) static buoyant force
bubble
F_b
liquid
R_p
particle
(c) hydrostatic pressure force
F_{hyd}
bubble
r_p
z_0
liquid
R_p
ω
particle
(d) capillary force
F_{ca}
bubble
γ
z_0
θ
liquid
R_p
ω
particle
(e) capillary pressure force
bubble
r_p
liquid
R_p
ω
F_σ
particle
(f) drag (detaching) force
bubble
liquid
R_p
particle
F_d

Figure 9

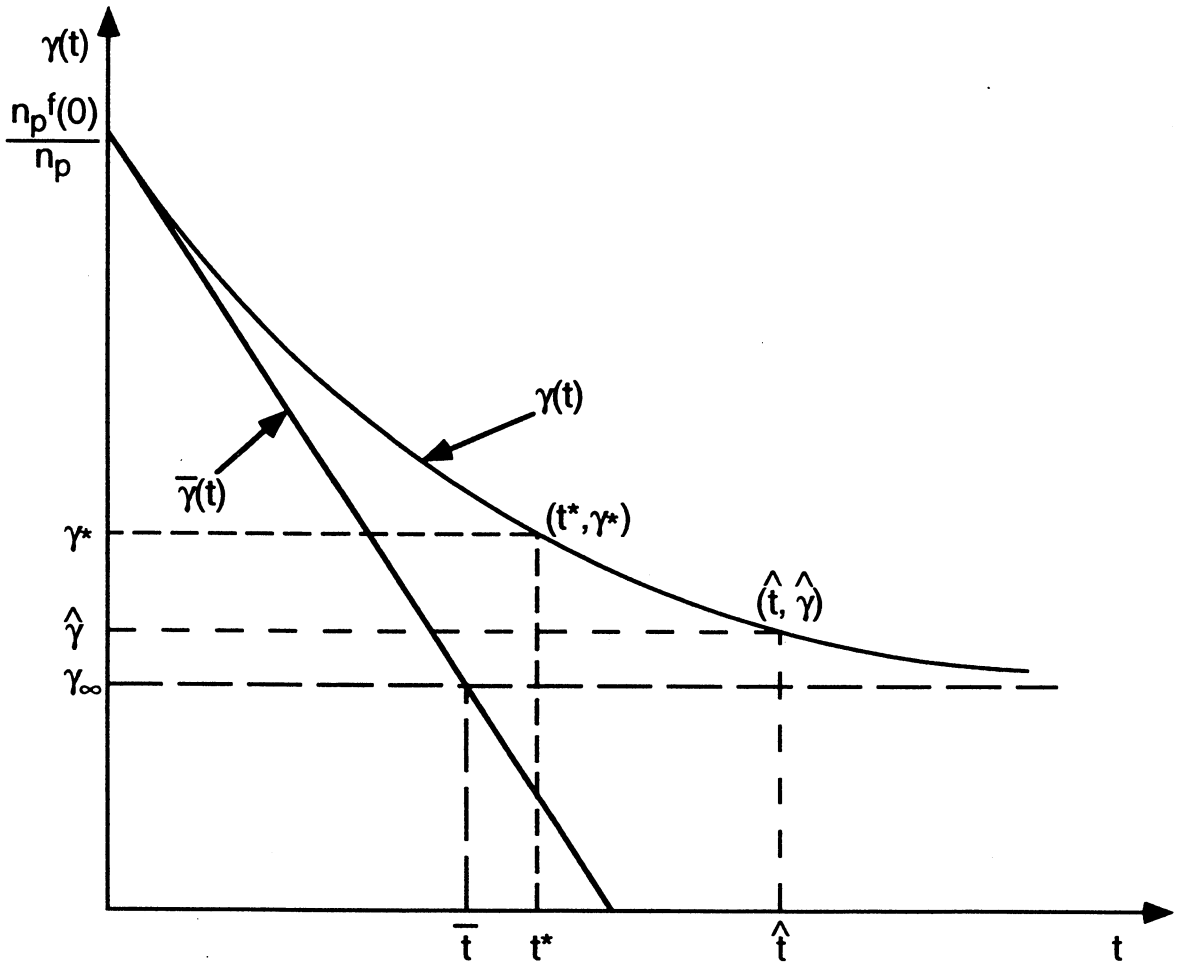
γ(t)
$\frac{n_p f(0)}{n_p}$
γ(t)
$\bar{\gamma}(t)$
(t*,γ*)
γ*
$(\hat{t}, \hat{\gamma})$
$\hat{\gamma}$
γ_∞
$\bar{t}$
t*
$\hat{t}$
t

Figure 10

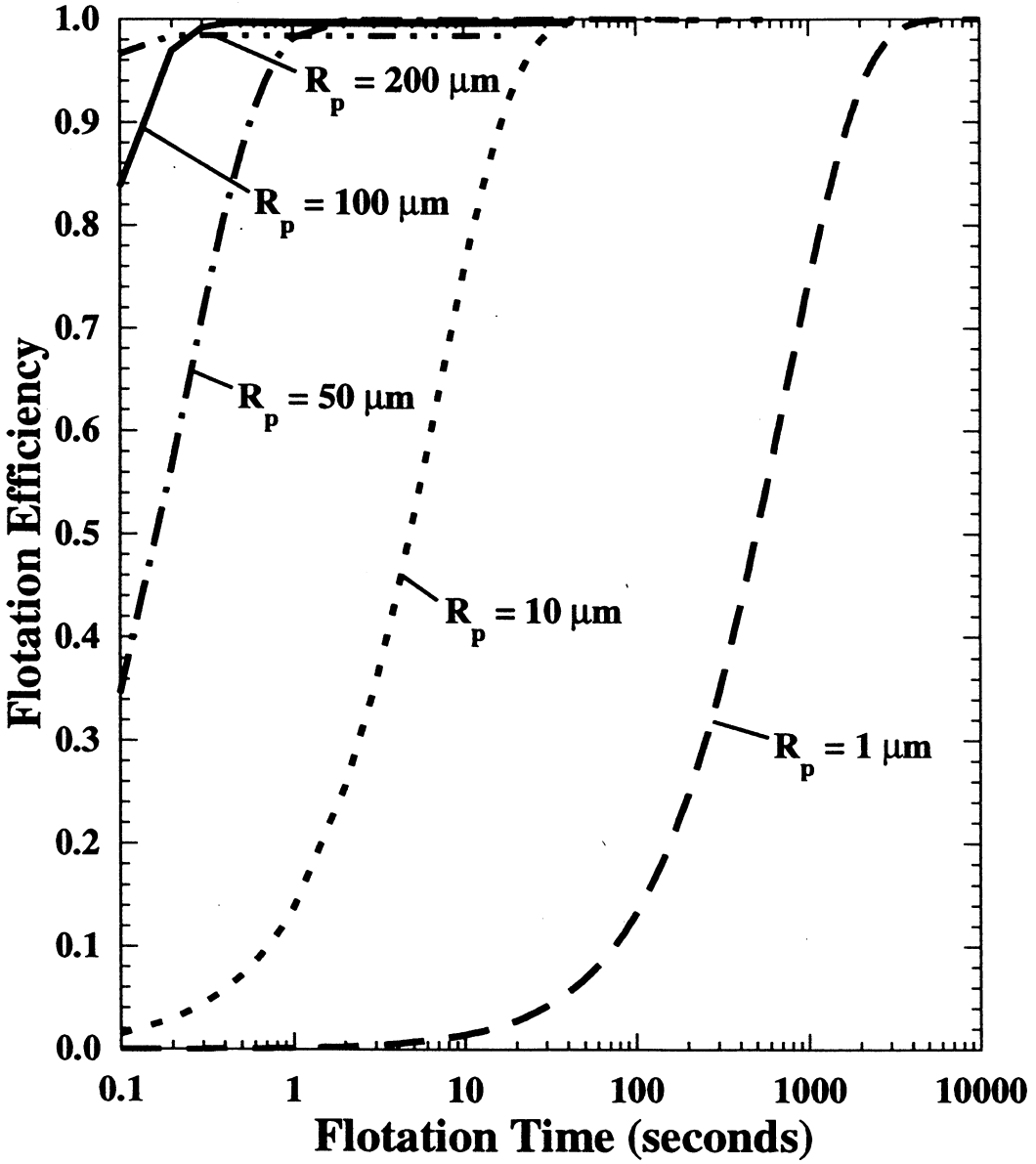
1.0
0.9
0.8
0.7
0.6
0.5
0.4
0.3
0.2
0.1
0.0
Flotation Efficiency
0.1
1
10
100
1000
10000
Flotation Time (seconds)
R_p = 200 μm
R_p = 100 μm
R_p = 50 μm
R_p = 10 μm
R_p = 1 μm

Figure 11

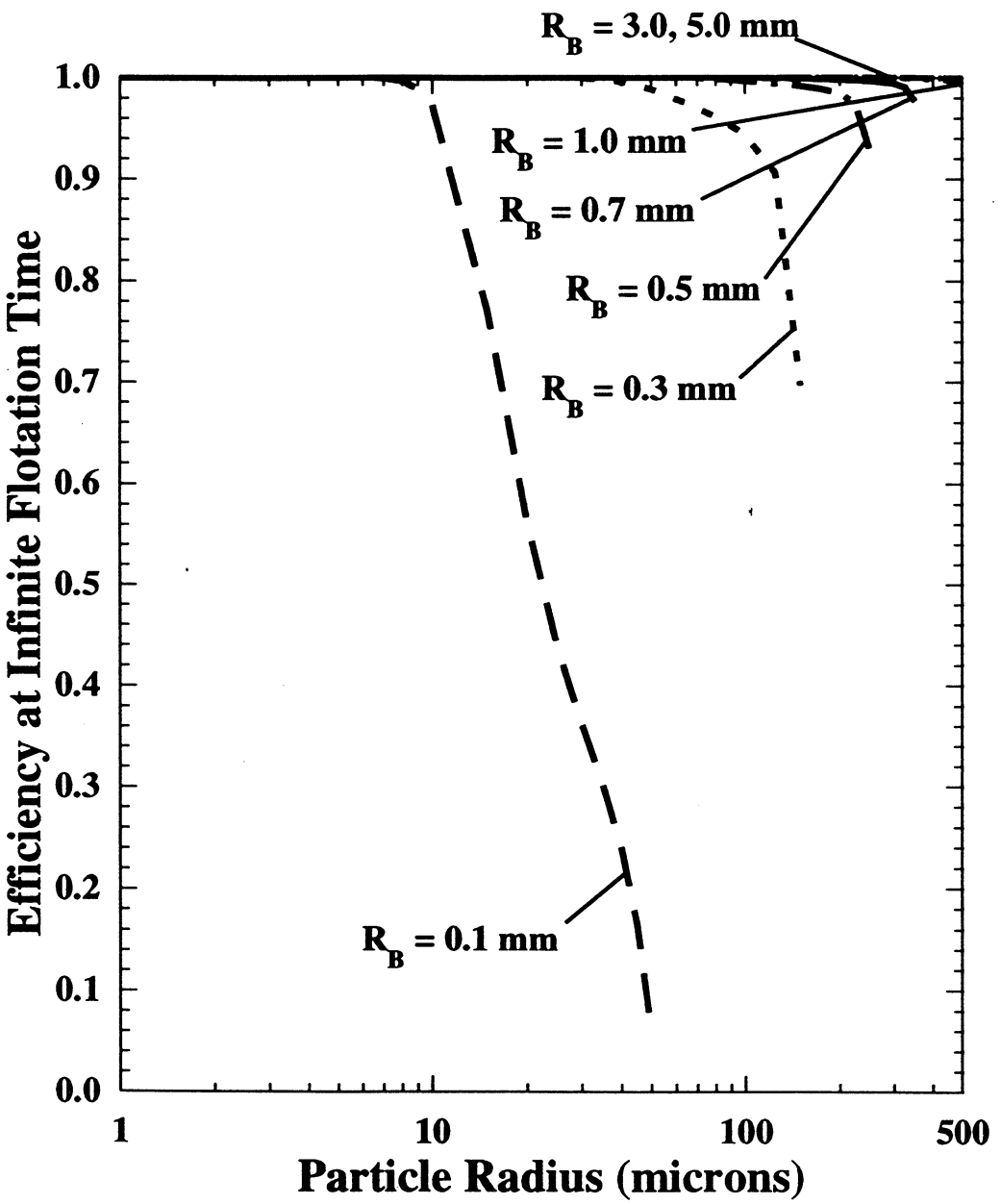
R_B = 3.0, 5.0 mm
R_B = 1.0 mm
R_B = 0.7 mm
R_B = 0.5 mm
R_B = 0.3 mm
R_B = 0.1 mm
Efficiency at Infinite Flotation Time
1.0
0.9
0.8
0.7
0.6
0.5
0.4
0.3
0.2
0.1
0.0
1
10
100
500
Particle Radius (microns)

Figure 12

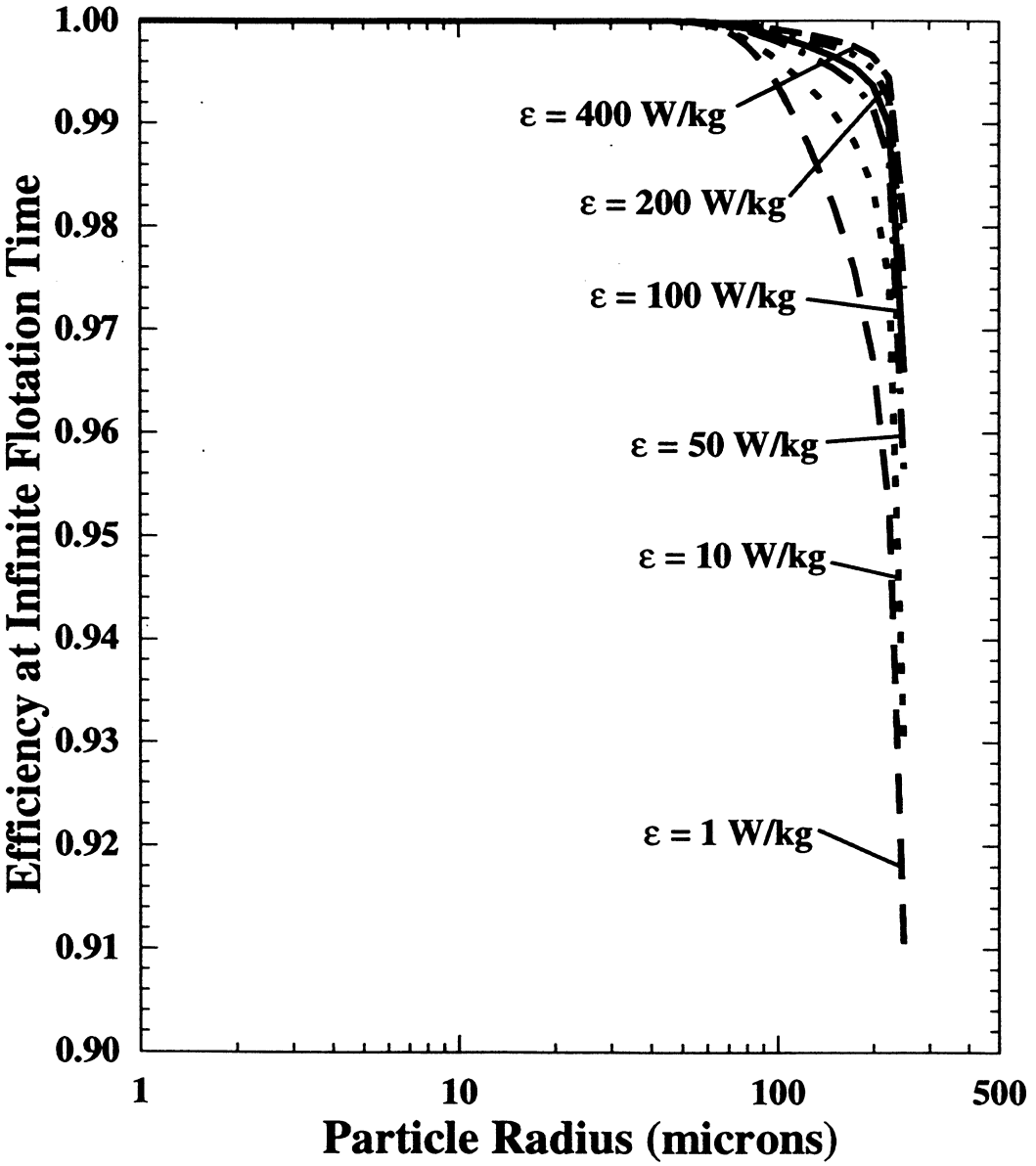
1.00
0.99
0.98
0.97
0.96
0.95
0.94
0.93
0.92
0.91
0.90
Efficiency at Infinite Flotation Time
ε = 400 W/kg
ε = 200 W/kg
ε = 100 W/kg
ε = 50 W/kg
ε = 10 W/kg
ε = 1 W/kg
1
10
100
500
Particle Radius (microns)

Figure 13

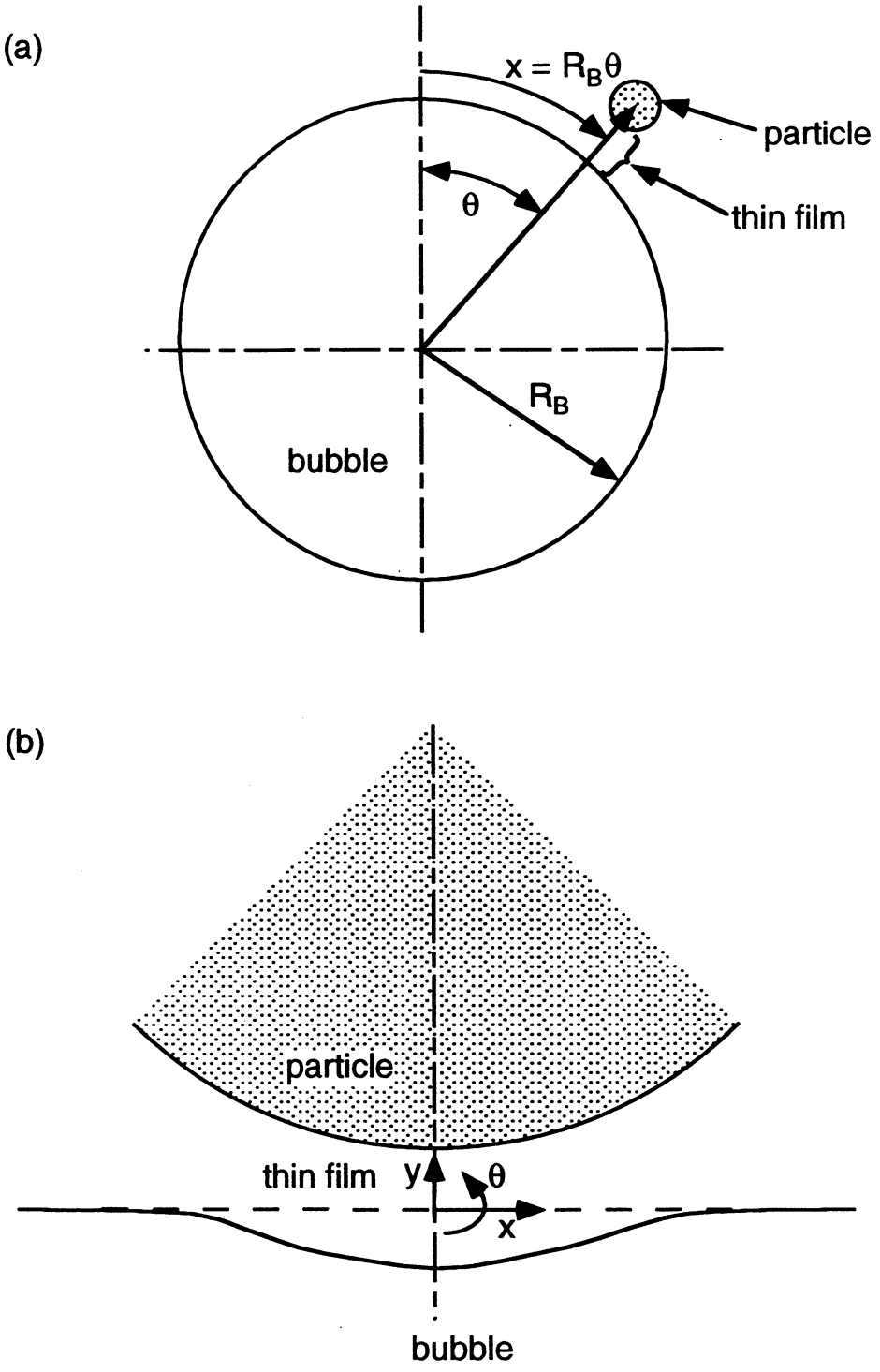
(a)
x = R_B θ
particle
thin film
θ
R_B
bubble
(b)
particle
thin film
y
θ
x
bubble

Figure 14